Geofísica Internacional (1994), Vol. 33, Num.3, pp. 399-420

Crustal structure of the eastern part of the Maya Terrane from magnetic anomalies and magnetic power spectrum inversion

J. García-Abdeslem[1] and G.E. Ness[2,3]

[1] *CICESE, División de Ciencias de la Tierra, Depto. de Geofísica Aplicada, Ensenada, B. C., México.*

[2] *College of Oceanography, Oregon State University Corvallis, Oregon, USA.*

[3] *Present address: Seafloor Surveys International, Inc., Seattle, Washington., USA.*

Received: March 9, 1993; accepted: September 13, 1993.

RESUMEN

Se interpreta una compilación reciente de anomalías magnéticas de campo total de la porción oriental del Terreno Maya, que incluye datos aeromagnéticos de la Península de Yucatán y datos magnéticos marinos de su margen continental hacia el norte y oriente. Con base en la amplitud, forma y extensión horizontal de las anomalías magnéticas y su correlación con información geológica y geofísica disponible se infiere que la porción oriental del Terreno Maya está constituída por al menos cuatro bloques tectónicos. Modelamos el espectro de potencia radial de las anomalías magnéticas de la margen continental al norte de la Península mediante la superposición de funciones que en forma estadística describen la profundidad a la cima, el espesor y las dimensiones horizontales de una colección de prismas verticales uniformemente magnetizados. Los resultados se exhiben en forma de mapas de contornos que muestran la profundidad a la cima y a la base de la corteza. El relieve del basamento promedia 1.8 km bajo el nivel del mar y está de acuerdo tanto con el carácter de las anomalías gravimétricas y magnéticas como con la interpretación de datos sísmicos y con información de pozos. La profundidad a la base de la corteza magnetizada varía de 15 a 35 km bajo el nivel del mar según la presencia o ausencia de anomalías magnéticas y gravimétricas de gran longitud de onda. Esta interpretación sugiere que localmente el *Moho* es la frontera magnética.

PALABRAS CLAVE: Anomalías magnéticas, inversión del espectro de potencia, estructura de la corteza, Terreno Maya, Bloque Yucatán, México.

ABSTRACT

We interpret a new compilation of total-field magnetic anomaly data from the eastern part of the Maya Terrane, comprising aeromagnetic data for the Yucatán Peninsula and marine magnetic data for its northern and eastern continental margins. Qualitatively, on the basis of amplitude, shape, and horizontal extent of the magnetic anomalies and their correlation with available geologic and geophysical information we infer that the eastern part of the Maya Terrane can be divided at least in four tectonic blocks. We model the radially-averaged power-density spectrum of the magnetic anomalies from the northern continental margin of the Yucatán peninsula by the superposition of functions that statistically describe the depth to the top and the thickness and horizontal dimensions of an ensemble of uniformly magnetized prisms. The results are portrayed as contour maps which show depth to basement and thickness of the crustal magnetic layer. The magnetic basement is found at an average depth of 1.8 km below sea level and shows some agreement with the character of magnetic and gravity anomalies, as well as seismic and drillhole data. The basal depth of the crustal magnetic layer varies from 15 to 35 km below sea level, in agreement with the presence or absence of long-wavelength magnetic and gravity anomalies. This interpretation suggests that locally the *Moho* is the magnetic boundary.

KEY WORDS: Magnetic anomalies, inversion of the power spectrum, crustal structure, Maya Terrane, Yucatán Block, Mexico.

INTRODUCTION

Large compilations of magnetic data over continental regions have proven useful to aid geologic mapping by providing information regarding the distribution of major rock units, for the estimation of depth to basement in sedimentary basins, and to estimate the depth extension of the crustal magnetic layer, which in a variety of geologic settings can be interpreted as the depth to the Curie-temperature isotherm. In this paper we examine a compilation of magnetic data from the Yucatán peninsula and its northern and eastern continental margins, and relate it to other geological and geophysical information. The mapped region, hereafter referred to as the Yucatán Block, is at the southeastern edge of the Gulf of Mexico Basin (Figure 1) and constitutes the easternmost portion of the Maya Terrane of Coney and Campa (1983). In the Yucatán block, carbonaceous and sedimentary rocks of Late Mesozoic and Cenozoic age overly a Paleozoic basement. It has been proposed that at the beginning of the Mesozoic, after the breakup of Pangea, seafloor spreading caused the Yucatán block to drift away from the Texas-Louisiana margin, to reach its present position at the end of Jurassic time (Pindel, 1985; Salvador, 1987).

Several geophysical studies have been conducted along the northern and eastern continental margins of the Yucatán Peninsula. The seismic refraction studies (Ewing *et al.*, 1960; Antoine and Ewing, 1963) in the northern margin showed a 2 km thick horizontally stratified sequence of Cenozoic and Upper Cretaceous sediments. Based upon single channel reflection studies, Dillon and Vedder (1973) described the eastern margin as consisting of elongated ridges and intervening basins parallel to the coast. More recently, Ibrahim *et al.*, (1981) carried out a refraction study with ocean bottom seismographs along the Campeche Terrace. They reported a seismic discontinuity at a depth of 14.58 km below sea level (BSL). A recent

interpretation of gravity and magnetic data (Alvarado-Omaña, 1986), based upon two-dimensional structures constrained with seismic and bathymetric data, has been carried out across the Campeche escarpment. The geophysical cross section by Alvarado-Omaña (1986) shows horizontally stratified layers up to 5 km thick overlying an upper crustal layer which bottoms at about 18 km depth, and overlies a lower crust where a horizontal crust-mantle interface is at about 32 km depth.

One of the aims of this work is to obtain an insight from the magnetic data interpretation into the yet unknown geometry of the deep crustal structure of the eastern part of the Maya Terrane, in order to help constrain the tectonic evolution of the tectonostratigraphic terranes of southern and eastern Mexico. In the first part of this work we examine the character of the total-field magnetic anomalies over the Yucatán Block, and we compare it with available gravity seismic and drillhole data. Based upon this qualitative inspection we infer the presence of at least four magnetic provinces. In the second part, we interpret the radially averaged power-density spectrum of magnetic anomalies in 34 grids of 128x128 km along the Campeche Bank from 21° to 26° of North latitude and from 86° to 93° of West longitude. In the interpretation of the spectra, we assume that the crustal magnetic field is due to one ensemble of vertical prisms, and we model the spectra by the superposition of functions that statistically describe depth, thickness and horizontal dimensions of prisms in the ensemble. We have used a method of inversion that is based on the ridge-regression algorithm. It depends on an initial set of parameters that is iteratively modified in order to reduce the misfit between the observed and the computed spectrum. The results are portrayed as contour maps that show estimates of the depth to basement and the thickness of the crustal magnetic layer.

GEOLOGICAL AND GEOPHYSICAL SETTING

The geologic history of the Yucatán Block plays an important role in modeling the origin and evolution of the Gulf of Mexico Basin. According to Salvador (1987), at the beginning of the Mesozoic, the area that would become the Gulf of Mexico Basin was occupied by a part of the supercontinent Pangea. The initial breakup of Pangea, during Late Triassic, was characterized by rifting and tensional deformation involving the stretching and thinning of the continental crust. This tectonic regime persisted until Middle Jurassic and generated rift grabens (Buffler, 1991; Salvador, 1987). It has been suggested that continuous rifting of Pangea caused the Yucatán Block to drift away from the Texas-Louisiana margin, that the Yucatán Block rotated approximately 43° in a counterclockwise sense with respect to a pole of rotation located in northern Florida, and reached its present position by the end of Jurassic time (Pindell, 1985, Salvador, 1987).

Several onshore holes drilled over the Yucatán Peninsula, and offshore at the Catoche knolls, have reached a variety of crystalline rocks comprising quartzites, schists, gneiss, granite, rhyolite, and andesite (Figure 1). López-Ramos (1975) reported that the PEMEX hole Yucatán No. 4, drilled in the Mérida area, recovered quartzite at a depth of 2390 m underlying the Todos Santos Redbed Formation. In Belize, the Basil Jones No. 1 drillhole reached schist at a depth of 2190 m, and the Tower Hill No. 1 hole reached granite at a depth of 2140 m. Near the center of the Yucatán Peninsula, the PEMEX Yucatán No. 1 drillhole found rhyolite at a depth of 3200 m, for which Rb-Sr dating indicates an age of 410 Ma (Silurian) and suggests a metamorphic event about 300 Ma ago (Mississippian) (López-Ramos, 1975). The Sacapuc and Chicxulub holes drilled by PEMEX in the Mérida area reach Cretaceous andesite at 1415 m and 1258 m depth (López-Rámos, 1975). Offshore (Figure 1) DSDP holes 537 and 538A bottomed in early Paleozoic metamorphic rocks. Schlager *et al.*, (1984) report that 200 m below sea floor, at 3000 m BSL, hole 537 recovered phyllite that records $^{40}Ar/^{39}Ar$ plateau ages of 500 Ma. About 300 m below the sea floor, at 2745 m BSL, hole 538A reached mylonitic gneiss and amphybolite, for which $^{40}Ar/^{39}Ar$ dates on hornblendes and biotite yielded 500 Ma. Several generations of diabase dikes feature whole-rock ages between 190 and 160 Ma (Schlager *et al.*, 1984).

The Paleozoic basement of the Yucatán Block is covered by a Late Triassic to Middle Jurassic rift assemblage of continental redbeds belonging to the Todos Santos Redbed Formation and the Evaporitas Yucatán Formation (López-Ramos, 1975; Viniegra-O., 1981). Overlying this rift assemblage is a sequence of shallow-water carbonates deposited since Late Cretaceous, which cover the Yucatán continental margin and the peninsula extending toward the western part of the Maya Terrane (Viniegra-O., 1981; Coney and Campa, 1983).

Following the general classification of Antoine and Ewing (1963), we have compiled the seismic velocities reported for the Campeche Bank. We group the seismic velocities into six units (Table 1). Correlation of seismic units with stratigraphic units was possible for the Chicxulub and Sacapuc holes drilled by PEMEX in the Mérida area. This correlation (Table 2) suggests that unconsolidated and consolidated sediments, ranging in seismic velocity from 1.7 to 2.4 km/s, were deposited since Late Tertiary (Miocene and Pliocene). Underlying these sediments is the Oligocene seismic unit A, which features sedimentary rocks of variable thickness and seismic velocity of 2.7-2.8 km/s. Early Tertiary (Eocene and Paleocene) and Late Cretaceous sediments are represented by seismic unit B, which ranges in seismic velocity from 3.1 to 3.8 km/s. Seismic unit C ranges in seismic velocity from 4.7 to 5.1 km/s, corresponding to Cretaceous andesite (5.1 km/s) in the Mérida area. The seismic unit D, reached underneath the Campeche Terrace, is deeper than the bottom of wells near Progreso. Its seismic velocity ranges from 5.6 to 5.9 km/s, which is in the range of measured values for the Paleozoic or Precambrian crystalline basement (Antoine and Ewing, 1963). The interface between seismic units C and D may correspond to the Middle Cretaceous Unconformity (Locker and Buffler, 1983; see also the Texas-Louisiana to Yucatán profile by Winker and Buffler, 1984). The seismic

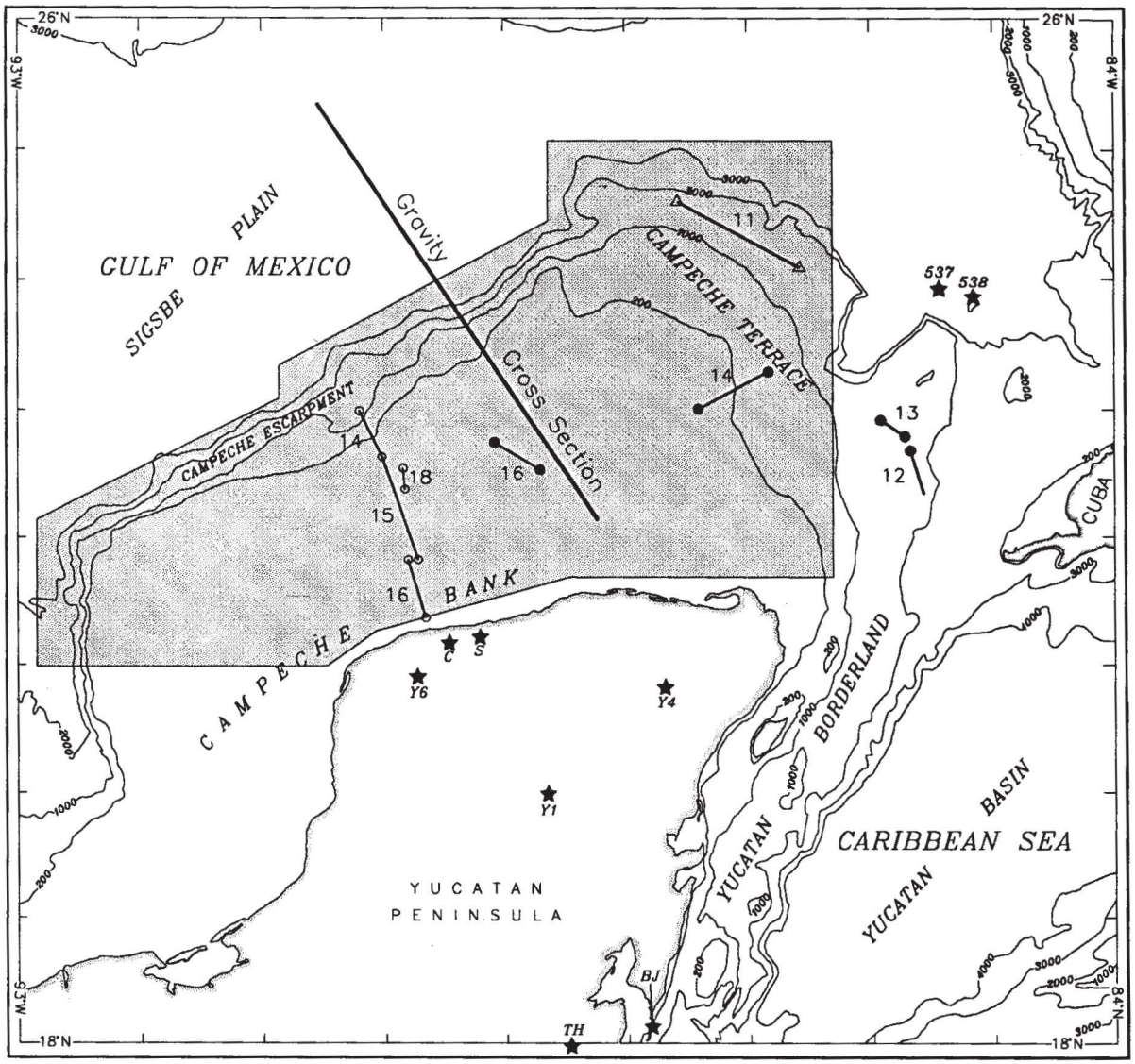

Fig. 1. Location map of the study area showing the location of drillholes where basement has been reached (Y-1=Yucatán No. 1, Y-2=Yucatán No. 2, Y-3=Yucatán No. 3, S=Sacapuc, C= Chicxulub, TH=Tower Hill, BJ= Basil Jones, 537 and 538 are from DSDP, Leg 77. Seismic profiles are denoted by solid circles (Ewing *et al.*, 1960), open circles (Antoine and Ewing, 1963), and with triangles (Ibrahim *et al.*, 1981). The geophysical cross section by Alvarado-Omaña (1986) is indicated. Bathymetric contours are in meters. Magnetic anomalies inside the grey polygon are used in this study to infer depth to magnetic sources and thickness of the crustal magnetic layer.

unit E with seismic velocity between 6.4 to 6.7 km/s corresponds to the lower crust.

Alvarado-Omaña (1986) used seismic refraction data by Ibrahim *et al.*, (1981) and gravity, magnetic, and bathymetric data from cruise Yucatán'85. His profile across the Campeche Escarpment (Figure 1) shows horizontal strata up to 5 km thick overlying an upper crust with a density of 2800 kg/m^3 which bottoms at about 18 km depth. His lower crust with a density of 3000 kg/m^3 extends down up to 32 km depth over a mantle of 3300 kg/m^3. He assumed a magnetic susceptibility of 0.0015 e.m.u. The top of the magnetic crust was interpreted as a highly irregular surface lying at depths between 3.5 to 13 km and its base as an horizontal surface at about 18 km below sea level beneath the Campeche Bank.

REGIONAL MAGNETIC PROVINCES

Marine magnetic data from the cruise Yucatán '85 (Ness *et al.*, 1991) and aeromagnetic data over the Yucatán peninsula from López-Ramos (1975) were used to produce a total-field magnetic anomaly map (Figure 2). The intensity of the earth's magnetic field in this region ranges from 45000 to 46000 nT; the declination is 4° east, and the inclination increases from 50° to 55° to the north.

Figure 3 describes the physiographic, structural, gravimetric, and magnetic features of the Yucatán block.

Valladolid Province. The Valladolid magnetic low (Figure 2), is about 100 km wide and extends to the north-

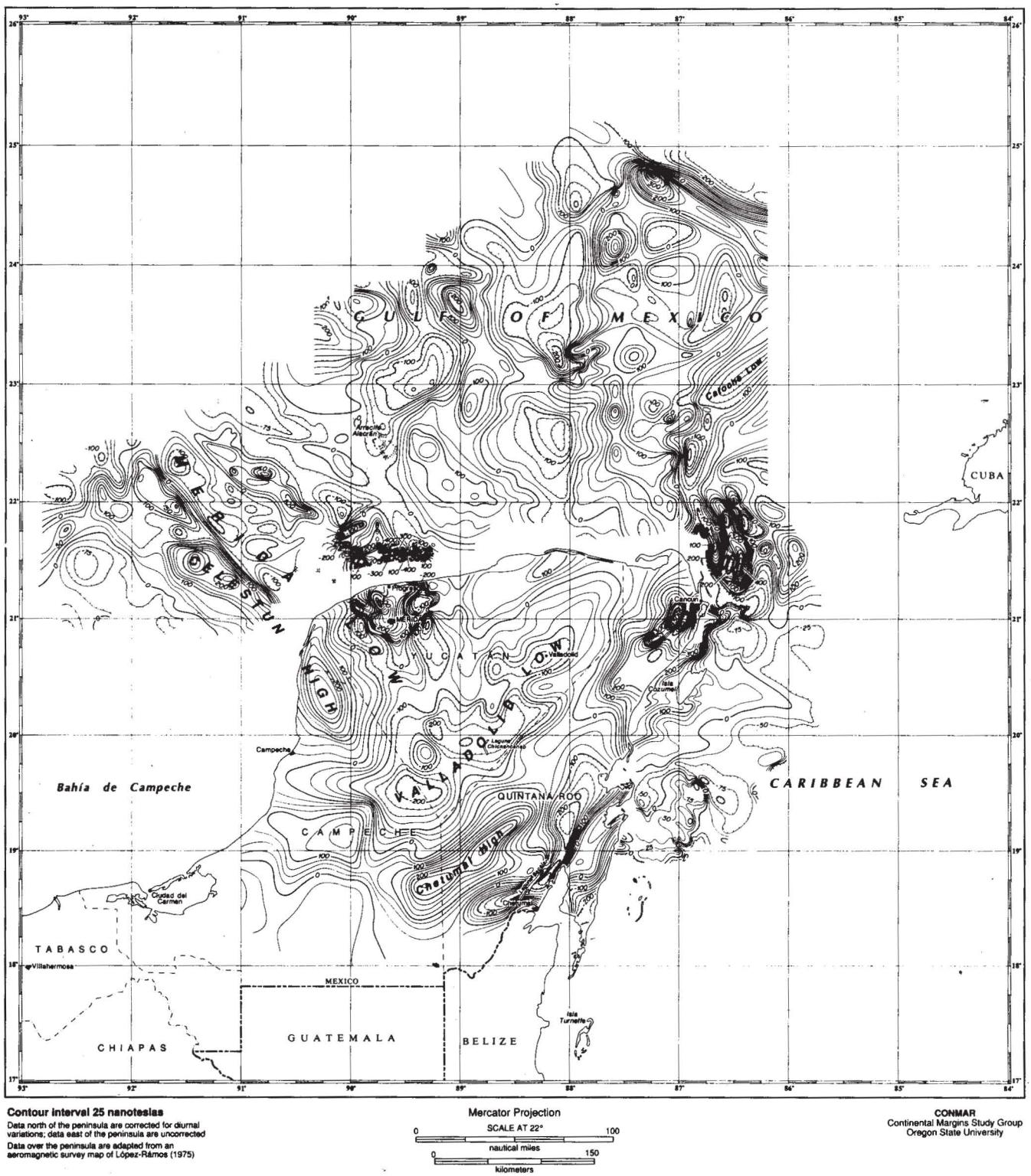

Fig. 2. Total field magnetic anomaly map of the Yucatán peninsula and adjacent areas. Aeromagnetic data from López-Ramos (1975) and marine magnetic data from Cruise Yucatán '85.

Table 1

Receiving positions, seismic velocities and layer thickness. Assumed velocities are indicated by asterisks and unreversed velocities by parentheses; all others are velocities determined by reversed profiles. The data sources are: (1) Ewing *et al.* (1960), (2) Antoine and Ewing (1963), and (3) Ibrahim *et al.* (1981).

Profile	Position		Velocity (km/sec)						Layer Thickness (km)					
	N.Lat.	W.Long.	Sediments	A	B	C	D	E	Water	Sediments	A	B	C	D
16SE[1]	22.533	88.733	2.3	(2.8)		4.8	5.7		.06		.54		2.2	
16NW	22.750	89.100							.06	.25	.40		1.1	
17[1]	22.750	89.100	2.1		3.1	4.8	5.7		.06	.17		.53	1.1	
14E[1]	23.283	86.850	2.0*		3.4	4.9		6.4	.73			1.9	1.4	
14W	23.000	87.417							.06	.10		.56	4.0	
13SE[1]	22.783	85.733	2.0*			4.9	5.9		1.38	.57			1.7	
13NW	22.917	85.933							.82	.25			3.1	
12[1]	22.633	85.700	2.0*			4.4	5.5	(6.7)	1.32	.29			2.5	7.0
16N[2]	21.833	89.817	1.9 - 2.4	2.7	3.6	5.1	5.7		.04	.21 - .17	.28	.63	.75	
16S	21.367	89.667							.01	.05 - .35	.31	.66	.50	
14A[2]	22.983	90.217	(2.0*)	(2.8*)	(3.8*)		5.6		1.46	.61	.37	.65		
14B	22.617	90.033												
15AN[2]	22.617	90.033	2.0 - 2.3	2.8	3.4	5.1*	5.8		.09	.23 - .24	.49	.46	.64	
15BS	21.817	89.733							.04	.22 - .19	.30	.46	.90	
17E[2]	22.517	89.667	1.7* - 2.3		3.4	4.9	5.9		.01	.09 - .73	.55	.47		
17W	22.550	89.833							.01	.10 - .70	.77	.50		
18S[2]	22.383	89.883	1.7* - 2.1		3.3	5.0	5.9		.01	.02 - .76	.63	.29		
18N	22.550	89.833							.01	.10 - .62	.74	.37		
11E[3]	24.130	86.640	2.0		3.4	4.7	5.9	6.4	1.28	.57		1.01	2.22	9.5
11W	24.610	87.590							.60	.01		.52	1.92	

Table 2

Correlation of seismic velocities from refraction station 16S of Ewing *et al.* (1963) with onshore geologic formations reported on holes Chicxulub, Sacapuc, and Yucatán-6 by López-Ramos (1975).

Seismic Unit	Velocity (km/sec)	Thickness (m)	Lithology and Geologic Age
		10	Water
	1.9	50	Caliche-Wackestone-Mudstone (Recent)
	2.4	350	Calcareous clay-Limestone (Miocene-Pliocene)
A	2.7	310	Calcareous clay-Shale-Limestone (Oligocene)
B	3.6	660	Limestone-Calcareous clay-Shale (Late Creataceous-Paleocene-Eocene)
C	5.1	500	Andesite (Cretaceous)
D	5.7		Metamorphic basement (Paleozoic ?)

east for more than 300 km. Within this regional low, several short-wavelength dipoles appear to be produced by normally-magnetized crust in the direction of the present field. The low amplitude of the magnetic anomalies, the coincidence of this magnetic province with the Valladolid gravity low (Figure 3), and the sedimentary thickness (3200 m) reported at the Yucatán No 1 drillhole all suggest a thick sedimentary basin overlying rhyolite and probably a Paleozoic basement. The abrupt change in direction of the gradient at the northeastern corner of the Copelchén magnetic high suggests either a faulted block in the southwest limit of the Valladolid province, or a basement of higher magnetic susceptibility.

Quintana Roo Province. This province is parallel to the Valladolid province. It includes the eastern part of Campeche State and all of Quintana Roo State. The most prominent magnetic anomalies in this province are Chetumal and Cancún-Mujeres. Both are positive anomalies that exceed 250 nT and extend for more that 100 km on a northeastern trend. A broad gravity high extends for 550 km, including all of Quintana Roo and extending about 100 km off Cancún. It reaches 100 mGal near the Cancún-Mujeres magnetic high. Gravity and magnetic data support the interpretation of a shallow basement under the eastern margin of the Yucatán Block.

Mérida-Celestun Province. This province includes northern Campeche and northwestern Yucatán. It extends offshore into the Campeche Bank, west of Alacrán Reef (Figure 2) and east of the Campeche Canyon (Figure 3). This region features a series of belts of alternating positive and negative anomalies extending for about 300 km in a northwest direction. The most prominent belts are the Mérida gravity and magnetic lows and the Banco Nuevo-Celestún gravity and magnetic highs. The elliptical region

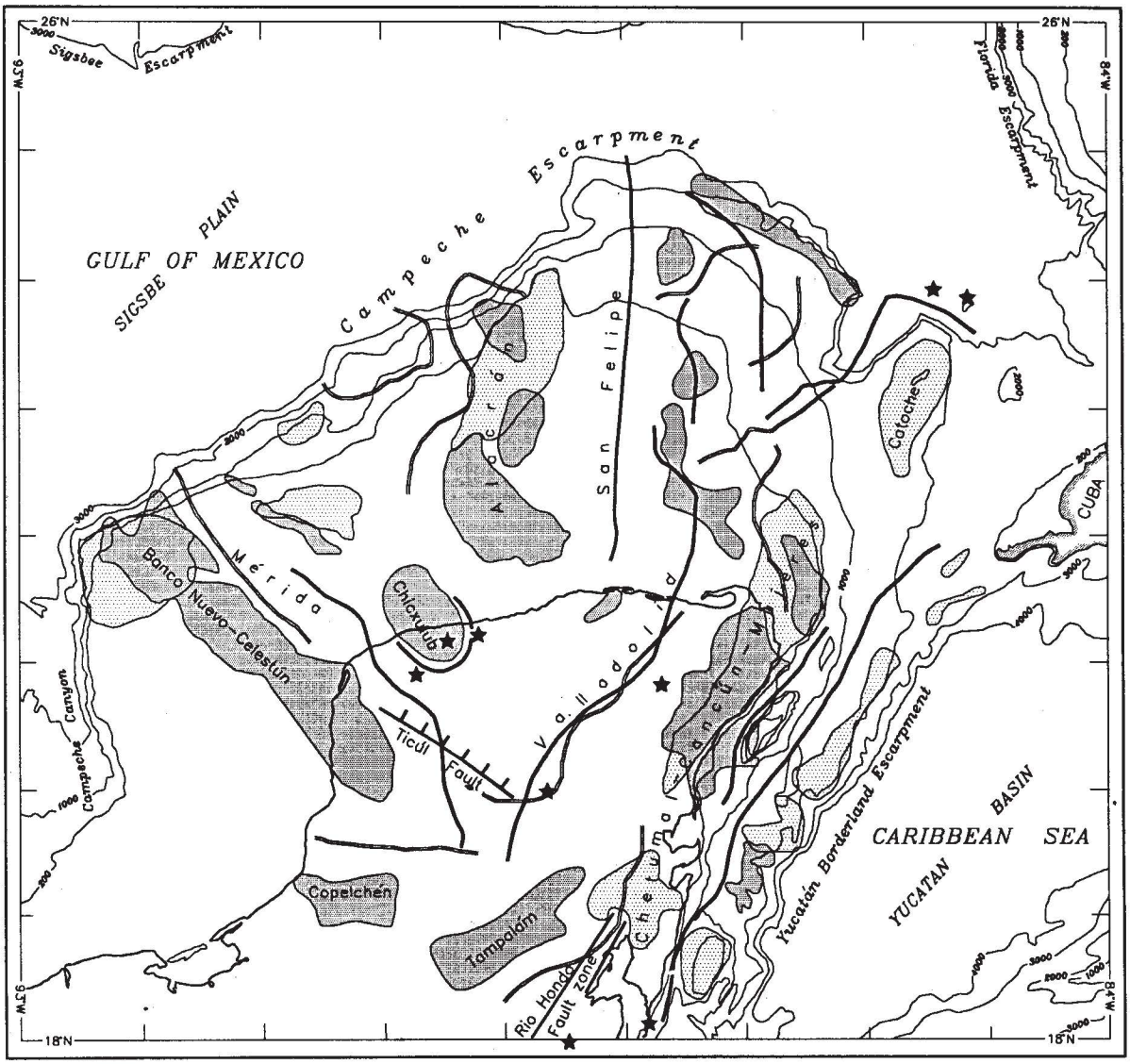

Fig. 3. Gravity and magnetic features of the Yucatán Peninsula and adjacent areas. Regions of positive magnetic (dots) and gravity anomalies (gray patterns) are shown. The axis of negative gravity and magnetic anomalies are denoted by solid and open lines.

surrounding Progreso features high-amplitude, short-wavelength magnetic anomalies attributed to a possible mid-plate igneous plume or to an astrobleme with associated extrusions (Penfield and Camargo, 1981; Hildebrand *et al.*, 1991).

San Felipe Province. This province encompasses anomalies offshore and east of the Alacrán Reef. The San Felipe lineament is a north-south magnetic low which extends along the 88°W meridian for more than 400 km (Figure 3). The Alacrán region to the west has long-wavelength magnetic highs and lows; its gradient overlaps the Alacrán gravity high. East of the San Felipe lineament we find intermediate wavelength (30 km) magnetic highs and lows lacking an obvious correlation with gravity. The San Felipe lineament may represent an edge effect of a structural boundary. The long-wavelength anomalies to the west may be due to deeply-seated magnetized rocks, while the short-wavelength anomalies to the east may represent sparsely distributed volcanic material.

MODELING AND INVERSION

The total-field magnetic anomaly f at a point outside a magnetic body is given by

$$f(\mathbf{r}) = \frac{\mu_0}{4\pi}\hat{\mathbf{B}}\cdot\nabla\left\{\int_v d^3s\ \mathbf{M}(\mathbf{s})\cdot\nabla\frac{1}{|\mathbf{r}-\mathbf{s}|}\right\} \quad , \qquad (1)$$

where **M** is the magnetization (*i.e.* the magnetic dipole moment per unit volume), **r** is the location of the observer, and **s** is the location of an element of volume of the source. The region V includes all of the magnetized material. The unit vector $\hat{\mathbf{B}}$ is in the local direction of the geomagnetic field, and μ_0 is the permeability of free space.

For a uniformly magnetized prism Eq. (1) may be written in the wavenumber domain (Bhattacharyya, 1966):

$$F(k,\theta) = \frac{\mu_0}{4\pi} M R_B(\theta;I,D) R_M(\theta;\phi,\lambda) \\ H(k;h)T(k;t)S(k,\theta;a,b) \quad . \qquad (2)$$

where k is the magnitude and θ is the direction of the wavenumber vector; M is the magnetic dipole moment per unit depth; $R_B(\theta) = \sin I + i \cos I \sin(D+\theta)$ where I is the inclination and D is the declination of the geomagnetic field; $R_M(\theta) = \sin\phi + i\cos\phi \sin(\lambda+\theta)$ for the inclination ϕ and declination λ of the magnetization vector; $H(k) = \exp(-hk)$ is the depth function, where h is depth to the top of the prism; $T(k) = 1 - \exp(-tk)$ is the thickness function, where t is the thickness of the prism; and $S(k,\theta) = sinc(ak_x \cos\theta/2)\ sinc(bk_y \sin\theta/2)$ is a function of the horizontal dimensions a and b of the prism.

We may generalize this result for an ensemble of rectangular vertical-sided prisms (García-Abdeslem and Ness, 1989; García-Abdeslem, 1990). The prisms are uniformly magnetized and randomly located in space. The ensemble is statistically characterized by a joint probability distribution Φ of the parameters of the prisms in the ensemble. Thus in the Fourier domain, the expected magnetic anomaly is

$$\langle F(k,\theta)\rangle = \int_v dR\Phi(h,t,a,b,M,\phi,\lambda,I,D)F(k,\theta) \quad , \qquad (3)$$

where the integration is carried out over the multidimensional parameter space R and over the local inclination and declination of the geomagnetic field. If the parameters in Eq. (3) vary independently, the probability of their joint occurrence is the product of their unconditional probabilities. In this case the integral can be separated and solved assuming a probability distribution for each parameter. Then

$$\langle F(k,\theta)\rangle = \frac{\mu_0}{2\pi}\langle M\rangle\langle R_M(\theta)\rangle\langle R_B(\theta)\rangle \\ \langle H(k)\rangle\langle T(k)\rangle\langle S(k,\theta)\rangle \qquad (4)$$

The product of $F(k,\theta)$ by its complex conjugate yields the power spectrum $E(k,\theta)$. A further simplification may be introduced by radially averaging the spectrum in order to eliminate its θ dependence, thereby transforming the two-dimensional spectrum into a one-dimensional spectrum. Thus

$$\langle E(k)\rangle = \left(\frac{\mu_0}{2\pi}\right)^2 \langle M\rangle^2\langle H(k)\rangle^2\langle T(k)\rangle^2 \\ \cdot \frac{1}{2\pi}\int_0^{2\pi} d\theta\, |\langle R_B(\theta)\rangle|^2 |\langle R_M(\theta)\rangle|^2 \langle S(k,\theta)\rangle^2 \quad . \qquad (5)$$

Assuming a uniform probability distribution for the magnetization strength and for the ensemble parameters the integration over θ yields

$$\langle E(k)\rangle = C_0\langle H(k)\rangle^2\langle T(k)\rangle^2\langle S(k)\rangle^2 \quad , \qquad (6)$$

where C_0 is a constant that contains I, D, ϕ, λ, and the mean magnetization of the prisms in the ensemble (García-Abdeslem, 1990). After radial averaging, the shape of the spectrum is independent of the direction of the local geomagnetic field and of the direction of magnetization. $\langle E(k)\rangle$ in Eq. (6) is indeed the solution of the forward problem; however, it is better to write it as the natural logarithm of the radially averaged and normalized power spectrum, *i.e.*

$$g(k) = \mathrm{Ln}\left[\langle H(k)\rangle^2\langle T(k)\rangle^2\langle S(k)\rangle^2\right] \quad . \qquad (7)$$

Different expressions of the radially-averaged power-density spectrum can be obtained by selecting different probability density functions for the ensemble parameters (García-Abdeslem and Ness, 1994). However, the magnetic data alone do not suffice to specify the best probability density function for a given ensemble, and thus it must be assumed. By trying different combinations of uniform and Gaussian distributions we settled for a normal distribution for the depth to the source top and a uniform distribution for the horizontal dimensions and the thickness; thus

$$\mathrm{Ln}\left[<H(k)>^2\right]=-2h_0k+k^2\sigma_h^2 \quad , \tag{8}$$

$$\mathrm{Ln}\left[<S(k)>^2\right]= \mathrm{Ln}\left\{\frac{1}{2\pi}\int_0^{2\pi}d\theta\left[\frac{Si(a_2)-Si(a_1)}{2\Delta a k\cos\theta}\right]^2\left[\frac{Si(b_2)-Si(b_1)}{2\Delta b k\sin\theta}\right]^2\right\}, \tag{9}$$

$$\mathrm{Ln}\left[<T(k)>^2\right]=2\mathrm{Ln}\left[1-\exp(t_0k)\frac{\sinh(k\Delta t)}{k\Delta t}\right] \quad . \tag{10}$$

Here h_0 is the mean depth to the top of the ensemble and σ_h^2 is the corresponding variance; t_0 is the average thickness of the prisms in the ensemble, and Δt is the range of thicknesses; *Si* is the sine integral, and

$a_1=(a_0-\Delta a)k\cos\theta$, $a_2=(a_0-\Delta a)k\cos\theta$,

$b_1=(b_0-\Delta b)k\sin\theta$, $b_2=(b_0\,\Delta b)k\sin\theta$,

where a_0 and b_0 are the mean horizontal dimensions, and Δa and Δb are the ranges in horizontal dimensions of the prisms in the ensemble.

We have data $(d_i, i=1,N)$, for only a finite number of wavenumbers $k_1,...,k_N$. Each d_i represents the averaged power within a concentric ring with respect to the spectral origin (*i.e.*, k=0), normalized with respect to the d.c. component of the spectrum. Similarly, each k_i represents the average position of the spectral components for a particular d_i.

In order to model our data, we need to find a group of parameters, m_j, $j=1,...,M$, such that the solution $g_j(\mathbf{m})$ to the forward problem fits the data within a prescribed threshold value. A solution to this inverse problem may be achieved through minimization of an objective function defined by

$$Q(\mathbf{m})=\sum_{i=1}^{N}\left[d_i-g_i(\mathbf{m})\right]^2 \quad . \tag{11}$$

To estimate **m** (the model parameters), the minimum of $Q(\mathbf{m})$ is sought. Because **g(m)** is nonlinear, the minimization must be achieved iteratively, by expanding **g(m)** about some initial trial $\mathbf{m}_0$ for the model parameters:

$$\mathbf{d}=\mathbf{g}(\mathbf{m}_0)+\partial\mathbf{g}(\mathbf{m})/\partial\mathbf{m}\,|_{\mathbf{m}_0}\,(\mathbf{m}-\mathbf{m}_0), \tag{12}$$

or more simply,

$$\mathbf{p}=\mathbf{A}\Delta\mathbf{m}, \tag{13}$$

where the vector $\mathbf{p}=\mathbf{d}-\mathbf{g}(\mathbf{m}_0)$ represents the error (or residual vector) between the observed and computed spectrum. **A** is an *(N, M)* matrix of partial derivatives of **g(m)** with respect to the model parameters, and the vector **Δm** represents the unknown perturbation which is to be added to the initial trial (*i.e.*, $\mathbf{m}_1=\mathbf{m}_0+\Delta\mathbf{m}$) in order to reduce the error. The partial derivatives with respect to depth and thickness were obtained analytically,

$$\frac{\partial g(k)}{\partial h_0}=-2k, \tag{14}$$

$$\frac{\partial g(k)}{\partial \sigma_h}=2\sigma_h k^2 \quad , \tag{15}$$

$$\frac{\partial g(k)}{\partial t_0}=\frac{2k\,\sinh(k\Delta t)/k\Delta t}{\exp(t_0k)-\sinh(k\Delta t)/k\Delta t'} \quad , \tag{16}$$

$$\frac{\partial g(k)}{\partial \Delta t}=\frac{2k\,\left[\sinh(k\Delta t)-k\Delta t\cosh(k\Delta t)\right]/(k\Delta t)^2}{\exp(t_0k)\;-\;\sinh(k\Delta t)/k\Delta t} \quad , \tag{17}$$

and the partial derivatives with respect to the horizontal dimensions were computed by finite differences.

To find **Δm** we use the ridge-regression algorithm (Marquardt, 1963):

$$\Delta\mathbf{m}=[\mathbf{A}^T\mathbf{A}+\lambda\mathbf{I}]^{-1}\mathbf{A}^T\mathbf{p}, \tag{18}$$

where **I** is the identity matrix and λ is a positive scalar quantity which is made to vanish during minimization in order to ensure stable convergence. The search for a minimum of $Q(\mathbf{m})$ is carried out starting from $\mathbf{m}_0$. It may end, after K iterations, at a local or absolute minimum for which $Q(\mathbf{m}_K)$ is within a prescribed threshold value. Upon convergence, the uncertainty of the source parameters may be estimated from

$$\sigma_{mj}=\sqrt{\sigma^2 a_{jj}} \quad , \tag{19}$$

where $\sigma^2=\mathbf{p}^T\mathbf{p}/(N-M)$ is the residual variance, *(N-M)* stands for the number of degrees of freedom, and $a_{jj}=\left[\mathbf{A}^T\mathbf{A}\right]^{-1}_{jj}$.

APPLICATION

The method described above was applied to the magnetic anomalies from the Campeche Bank. The diurnally corrected marine magnetic data were gridded using the minimum curvature algorithm of Briggs (1974), at a sampling interval of 1 km on a Universal Transverse Mercator projection, over an area of 21° N to 26° N, and 86° W to 93° W. The gridded data were divided into 34 square sub-grids 128 km wide and with a 50% overlap. Each sub-grid was detrended to remove the mean and the trend by taking out the first-order surface of best fit to the data in the least-squares sense. Edges of sub-grids were tapered by applying a 10 point cosine bell to damp out the discontinuities at the edges, and the nodes beyond the grid edges were filled with zeros to obtain sub-grids of 256x256 samples.

For each subgrid a two-dimensional Fourier transform was computed; power spectra were calculated and reduced to one-dimensional spectra by averaging over concentric rings about k=0, and normalizing with respect to the d.c. values. The natural logarithm of each one-dimensional power-density spectrum was obtained and the new "data" were expressed as a function of inverse wavelength.

The purpose of this exercise is to examine the statistical properties of the patterns of magnetic anomalies. In particular, we wish to estimate depth to basement and thickness of the magnetic crust in the northern continental margin of the Yucatán Peninsula. We modeled the Yucatán spectra assuming a Gaussian probability distribution of the depth to the top of the prisms in the ensemble, and uniform probability distributions for the horizontal dimensions and the thickness of the prisms. The system of equations (18) was solved by Choleski decomposition, using an initial value of λ =1 for the damping parameter. The results are summarized in Table 3. The observed and computed spectra are shown in Appendix A. Estimated depths to the basement and to the base of the crustal magnetic layer are assigned to grid centers (Figure 4) and contoured on top of the bathymetry. Of course these contour maps are based on very few (34) depth estimates and can only give a broad, regional indication of the true depth to the various horizons. The contour maps include seismic velocity (Table 3) and estimates of depth to the crust-mantle interface (Alvarado-Omaña, 1986); they may be compared with the compilation of significant gravity, magnetic and structural features shown on Figure 3.

RESULTS AND DISCUSSION

Depth to the top of the crustal magnetic layer

Figure 5 is a 200 m contour map of mean depths to the magnetic basement. The depths range from 1400 to 3000 m BSL. Off Progreso this horizon lies between 1440 to 1600 m, which is consistent with the depth at which andesites were reached in holes Chicxulub (1415 m) and Sacapuc (1258 m). North of Progreso and west of Alacrán Reef this horizon consistently lies within the 5.1 km/s seismic unit C, which corresponds to andesites found at holes Yucatán No. 6, Sacapuc, and Chicxulub.

Northeast of Progreso is a region featuring long-wavelength positive magnetic anomalies but negative free-air gravity anomalies. Contours of the magnetic basement suggest the presence of an elliptical basin where a 2 km thick sedimentary cover overlies this horizon. North of this elliptical feature and east of Alacrán Reef the magnetic basement shallows to 1600 m BSL; this horizon matches magnetic anomalies of dipole signature as well as the southwestern edge of the Alacrán gravity high. Towards the western Campeche Bank, in the Mérida-Celestún magnetic province which features short-wavelength magnetic anomalies, this horizon lies about 1800 m BSL.

Along the Campeche Terrace, following the offshore extension of the Cancún-Mujeres gravity high which features a complex pattern of intermediate-wavelength magnetic anomalies, this horizon suggests two basins separated by a basement high. West of Catoche Peninsula near refraction leg 14 (Figure 1), this horizon is within the 4.9 km/s seismic unit C. It deepens eastward, in agreement with the thickening of the 3.4 km/s seismic unit B.

The base of the crustal magnetic layer

Depth and thickness estimations were added to obtain the depth to the base of the crustal magnetic layer. The result is shown in Figure 6 as a 2500 m contour map. This horizon can be interpreted either as a lithologic boundary between magnetic material on top of non-magnetic material, or as the depth to the Curie isotherm.

Northwest of Progreso, in the region of the Mérida-Celestún magnetic province, this horizon rises to 17 km BSL. The trend of magnetic anomalies and the absence of long wavelength gravity and magnetic anomalies both agree with the shallow depth of the base of the crustal magnetic layer in this area. The shallowest feature in this horizon, 15 to 17.5 km BSL, occurs west of Catoche Peninsula across the intra-shelf escarpment that separates the Bank of Campeche from Campeche Terrace. This feature deepens and extends southward to the offshore extension of the Isla Mujeres gravity high.

East of Alacrán Reef the base of the magnetic layer ranges between 27.5 and 35 km BSL which is close (within 1.5 km) to the crust-mantle boundary determined by Alvarado-Omaña (1986) from two-dimensional modeling of free-air gravity anomalies. Thus in this particular region, the Moho may be the magnetic boundary. Along the western Campeche Terrace, the depth to the base of the magnetic layer is on average 30 km BSL. Alvarado-Omaña (1986), using the velocity structure by Ibrahim *et al.* (1981), found the crust-mantle interface at a depth of 28 km BSL. This result is consistent with our findings and suggests that the Moho is the magnetic boundary also in this region.

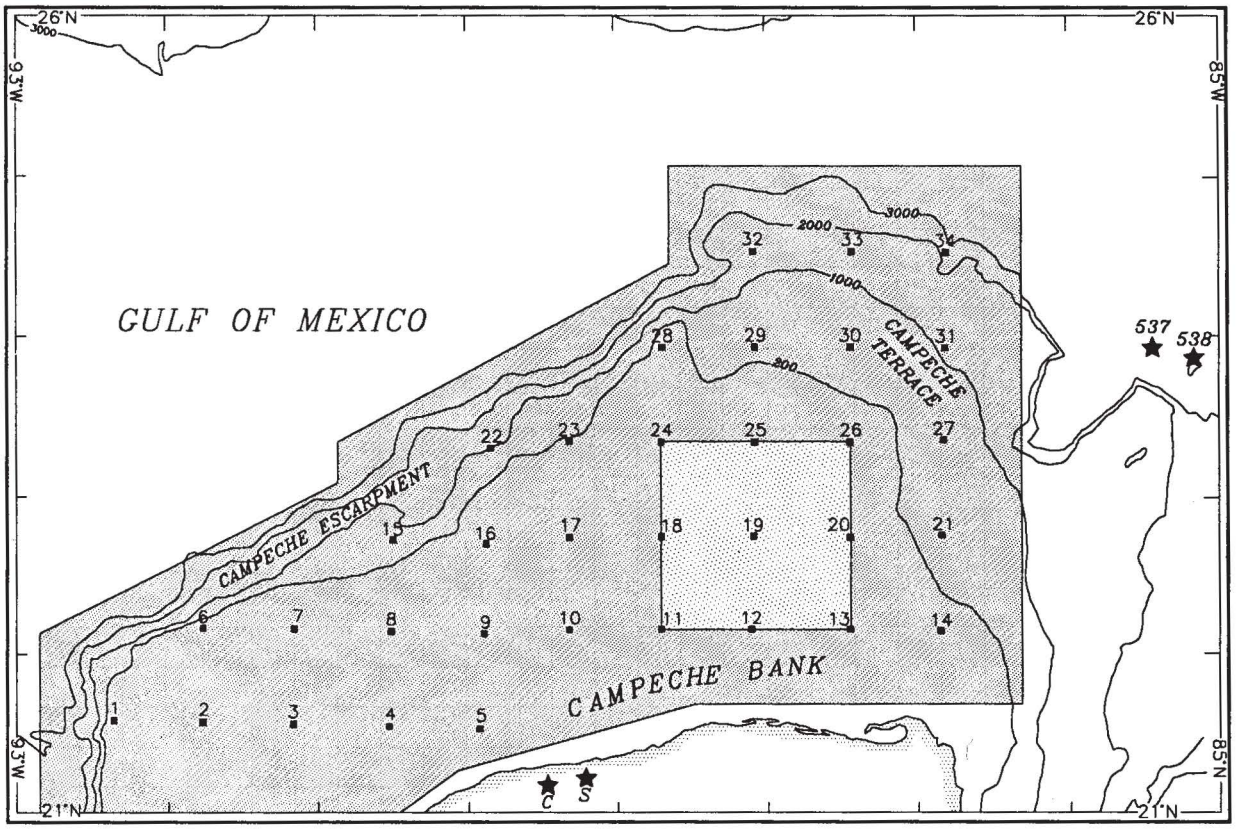

Fig. 4. Location of sub-grid centers. The size of sub-grid 19 is indicated.

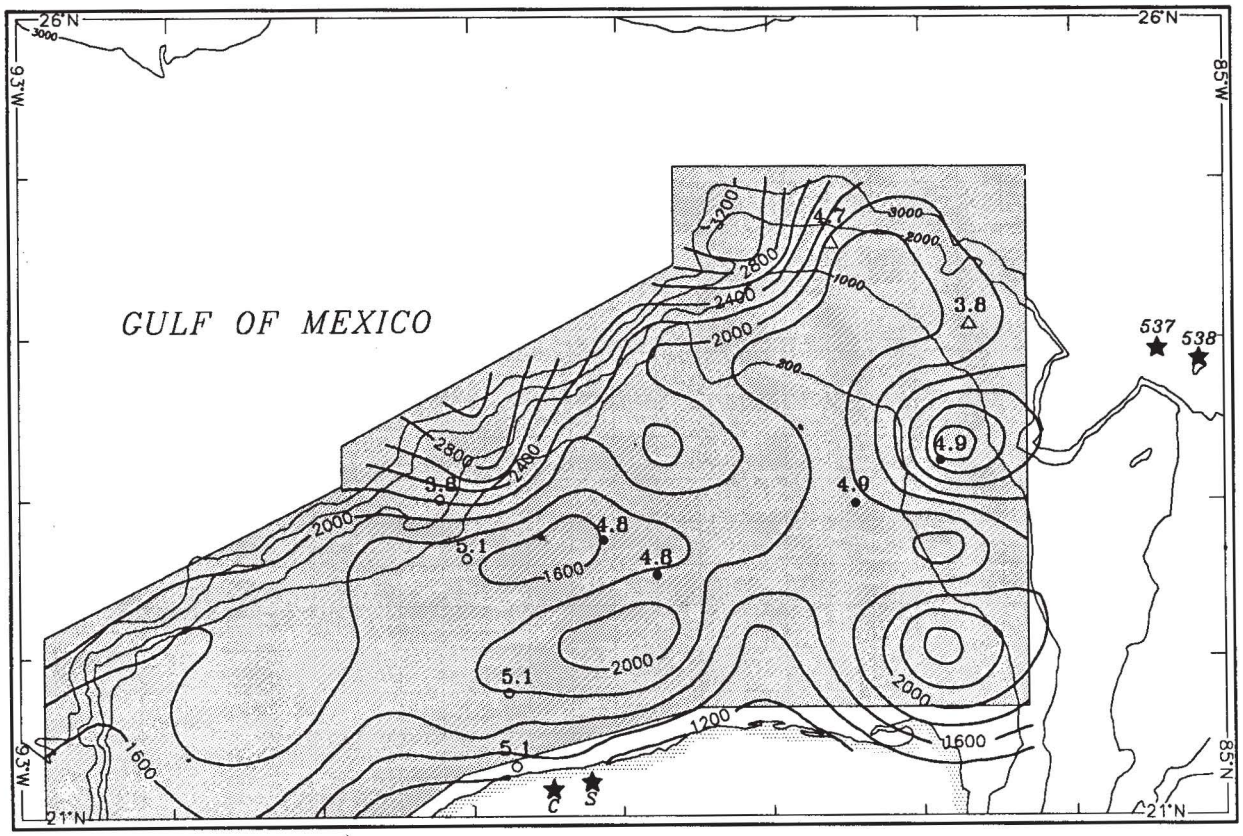

Fig. 5. Contour map of depth to the top of the magnetic basement, determined by ridge-regression inversion of the power spectrum of magnetic anomalies, and seismic velocities at the depth of the same.

Table 3

Results of the ridge-regression inversion of the Yucatán spectra. Units are in km and uncertainty in all parameters is as in equation (19).

Grid	h_0	σ_h	t_0	a_0	Δa	b_0	Δb	C_0	Q(m)
1	1.58±.05	0.81±.02	32.38±3.14	18.27±.14	16.86±.07	16.65±.08	14.40±.08	13.12±.74	4.83
2	1.91±.05	0.88±.01	25.01±2.29	18.58±.14	17.19±.07	16.58±.15	14.37±.08	3.33±.07	4.58
3	1.87±.06	0.85±.02	23.42±2.34	19.90±.16	18.56±.08	17.79±.18	15.63±.10	4.65±.08	5.58
4	1.50±.13	0.85±.02	17.55±2.91	17.37±.30	16.83±.11	11.87±.27	9.52±.16	4.77±.16	16.25
5	1.63±.08	0.73±.04	24.37±3.34	19.78±.22	18.40±.12	17.81±.25	15.60±.14	3.90±.11	10.27
6	1.77±.05	0.81±.02	21.05±1.77	18.82±.14	17.47±.08	16.89±.15	14.72±.08	4.79±.07	3.97
7	1.96±.05	0.87±.02	16.89±1.34	18.68±.10	17.59±.05	16.79±.18	15.03±.09	4.17±.07	4.20
8	1.74±.16	0.60±.09	16.52±3.15	20.59±.05	19.80±.03	14.89±.16	12.25±.09	9.38±.18	21.82
9	1.71±.82	0.68±.21	22.89±3.31	13.57±1.74	13.24±.81	13.14±.53	12.95±.58	3.50±.16	9.38
10	2.05±.10	0.86±.07	27.93±3.36	17.75±.54	17.43±.17	16.54±1.64	14.44±.89	3.14±.11	7.11
11	2.17±.21	0.87±.05	23.99±2.92	20.27±.86	17.43±.17	16.07±1.71	13.83±.93	2.69±.13	6.90
12	1.34 ±.07	0.89±.05	28.31±3.88	18.74±.21	17.42±.10	16.85±.24	14.66±.13	3.56±.11	10.03
13	1.76±.07	0.89±.05	20.53±2.08	19.09±.13	18.03±.05	17.39±.24	15.61±.11	2.36±.08	6.41
14	2.57±.11	0.84±.03	15.26±1.91	22.84±1.22	22.89±.62	9.75±.54	7.29±.29	4.49±.14	8.57
15	1.73±.08	0.60±.09	16.11±1.68	19.18±.13	18.14±.06	17.63±.24	15.91±.16	3.75±.09	6.89
16	1.62±.08	0.73±.03	26.13±3.55	18.54±.19	17.17±.10	17.90±.26	15.71±.14	3.79±.11	9.99
17	1.45±.05	0.69±.02	32.84±3.34	19.94±.16	18.60±.80	17.73±.18	15.56±.99	3.89±.08	5.33
18	1.70±.08	0.78±.03	31.50±4.44	18.40±.20	17.02±.11	17.68±.24	14.45±.13	3.76±.11	10.29
19	1.88±.06	0.81±.02	19.91±2.18	18.95±.17	17.64±.09	17.11±.20	14.98±.11	3.27±.10	6.91
20	1.62±.06	0.65±.03	13.18±1.32	19.83±.16	18.62±.07	18.00±.20	15.95±.11	3.26±.10	5.95
21	1.41±.04	0.56±.02	27.30±2.32	19.99±1.25	18.85±.05	18.22±.18	16.25±.09	3.03±.06	4.06
22	3.20±.33	1.12±.04	21.32±3.61	23.29±1.07	23.20±.83	18.86±2.54	17.17±1.35	3.20±.22	9.99
23	1.94±.07	0.84±.03	34.01±4.39	18.55±.21	17.16±.12	17.24±.23	15.03±.13	3.65±.10	8.47
24	2.31±.10	0.96±.03	22.01±3.42	17.67±.29	15.42±.16	18.16±.22	16.73±.12	3.98±.14	13.28
25	1.98±.07	0.81±.02	18.87±2.12	19.69±.18	18.39±.09	17.91±.22	15.77±.12	3.19±.10	7.32
26	1.76±.07	0.69±.11	17.60±2.11	18.49±.29	16.38±.16	16.88±.16	15.64±.11	3.16±.11	8.57
27	2.97±.10	0.12±.03	10.81±1.00	19.86±.05	19.41±.06	16.86±.58	15.34±.30	4.96±.13	2.76
28	1.91±.07	0.86±.03	23.79±2.68	17.25±.15	15.84±.08	17.52±.21	15.30±.12	3.39±.09	6.93
29	1.64±.05	0.69±.02	32.29±3.31	18.28±.14	17.03±.06	17.76±.21	15.69±.11	2.82±.08	5.52
30	1.75±.05	0.70±.07	32.14±3.49	18.03±.14	16.78±.07	17.76±.22	15.69±.12	3.75±.08	6.22
31	1.87±.06	0.77±.02	20.82±2.07	17.15±.13	15.82±.07	16.70±.19	14.53±.11	5.68±.09	5.64
32	3.03±.15	1.17±.04	26.88±3.36	19.46±.05	18.71±.05	17.45±.13	15.98±.06	5.03±.12	7.13
33	1.63±.06	0.68±.03	26.30±2.78	18.80±.16	17.51±.08	17.04±.19	14.91±.10	2.53±.08	6.11
34	1.97±.07	0.79±.03	28.11±3.50	19.97±.20	18.60±.10	17.86±.22	15.65±.12	2.96±.10	8.28

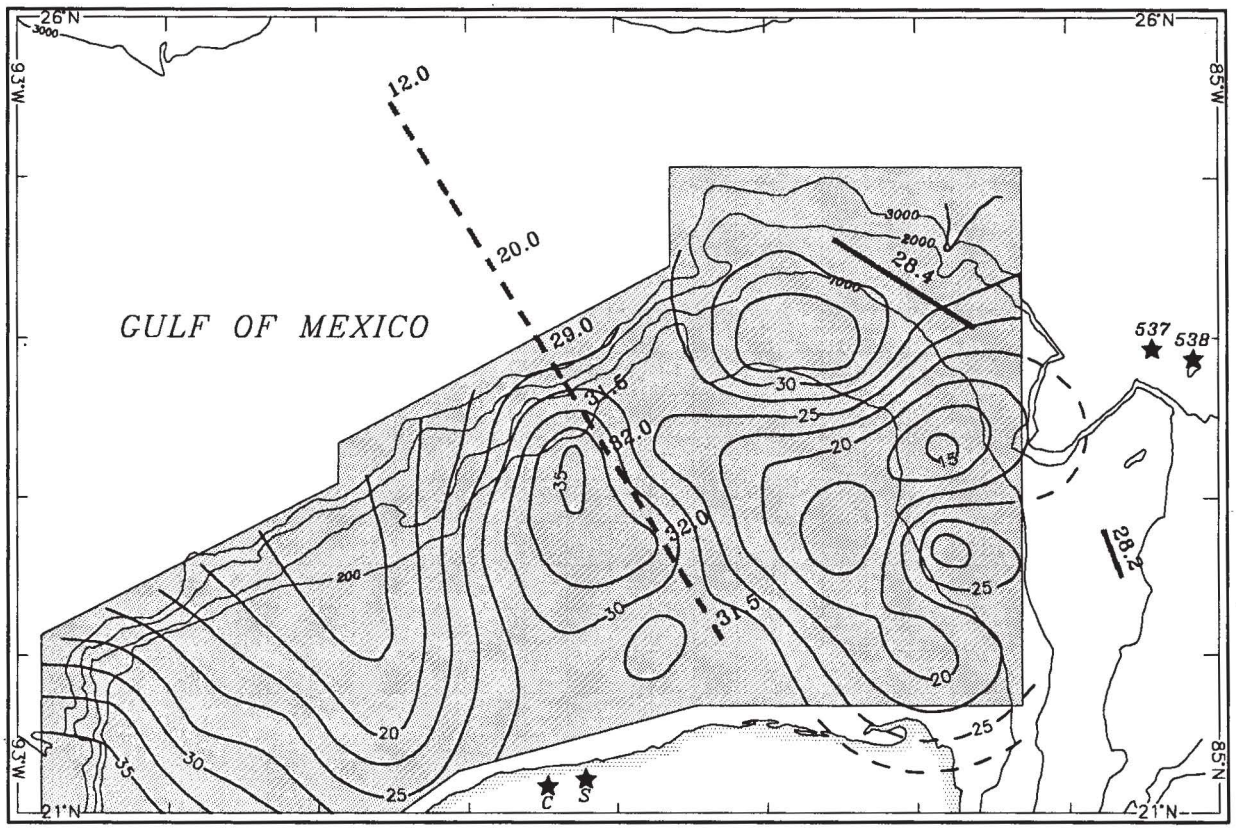

Fig. 6. Contour map of depths to the base of the crustal magnetic layer, determined by ridge-regression inversion of the power spectrum of magnetic anomalies. Depths to the crust-mantle interface as inferred from gravity modeling and mass column analysis are also shown.

CONCLUSIONS

We present a new compilation of magnetic anomalies based on aeromagnetic data from the Yucatán Peninsula and marine magnetic data north and east of the continental margin. On the basis of amplitude, shape, and horizontal extent of the magnetic anomalies, we propose that the Yucatán Block can be divided in at least four magnetic provinces. The boundaries between provinces appear as long linear magnetic features extending for several hundreds of kilometers between regions with different magnetic and gravity signatures. Each province may correspond to a different tectonic block. This interpretation is in agreement with Coney and Campa (1983), who propose that the eastern Maya Terrane is a composite Terrane.

The crustal magnetic field is modeled as a particular realization of an ensemble of uniformly magnetized and randomly distributed vertical prisms. The radially-averaged power-density spectrum is obtained by the superposition of functions that statistically describe depth to the top of the source, thickness, and horizontal dimensions of the source. This new approach was applied to an analysis of the total-field magnetic anomalies from the northern continental margin of the Yucatán Peninsula. Depth and thickness estimations from the Yucatán spectra were used to construct contour maps of the mean depth to the top of the magnetic basement and thickness of the crustal magnetic layer.

The magnetic basement is at an average depth of 1.8km BSL. The seismic velocity at this depth ranges between 4.8 and 5.1 km/s along the Campeche Bank, and between 4.9 to 3.4 km/s along the Campeche Terrace. Off Progreso, the depth to this horizon is within the range of depths reported for andesites at holes Sacapuc, Yucatán No. 6, and Chicxulub. The computed depth to the base of the crustal magnetic layer is highly variable. It fluctuates between 15 and 35 km BSL. The shallowest base is found along the eastern part of the margin, and along the western part of the margin, suggesting that important changes in magnetization occur in the lower crust. These two regions are separated by thick blocks, where the depth to the base of the crustal magnetic layer lies at about 30 km BSL. The thickness of the crustal magnetic layer east of Alacrán Reef and along the eastern part of the Campeche Terrace is consistent with the depth to the crust-mantle boundary as determined from seismic and gravity data modeling. In these regions the Moho is the magnetic boundary.

ACKNOWLEDGMENTS

We acknowledge the valuable comments on earlier versions of this paper made by Richard W. Couch, J. Paul Dauphin, C.F. Flores Luna and L.A. Delgado Argote. Cri-

tical reviews and suggestions by two anonymous reviewers and by the senior editor are appreciated. We thank J.E. Bowers for technical support during data collection. We also acknowledge the support from Admiral Gustavo Calderón Riveroll and the assistance of the crew and captain J.R. Alcalá Pigñol of R/V Altaír (Mexican Navy). Figures were drafted with the help of S. Troseth, M. Almeida Vega, and V.M. Frías Camacho.

APPENDIX A

Figures A1 to A34 show the radially-averaged power-density spectra computed from magnetic anomalies in the Yucatán northern continental margin, and the artificial spectra obtained by ridge-regression inversion. In each figure, the field-data spectra are represented by circles. The artificial spectra are shown as continuous lines.

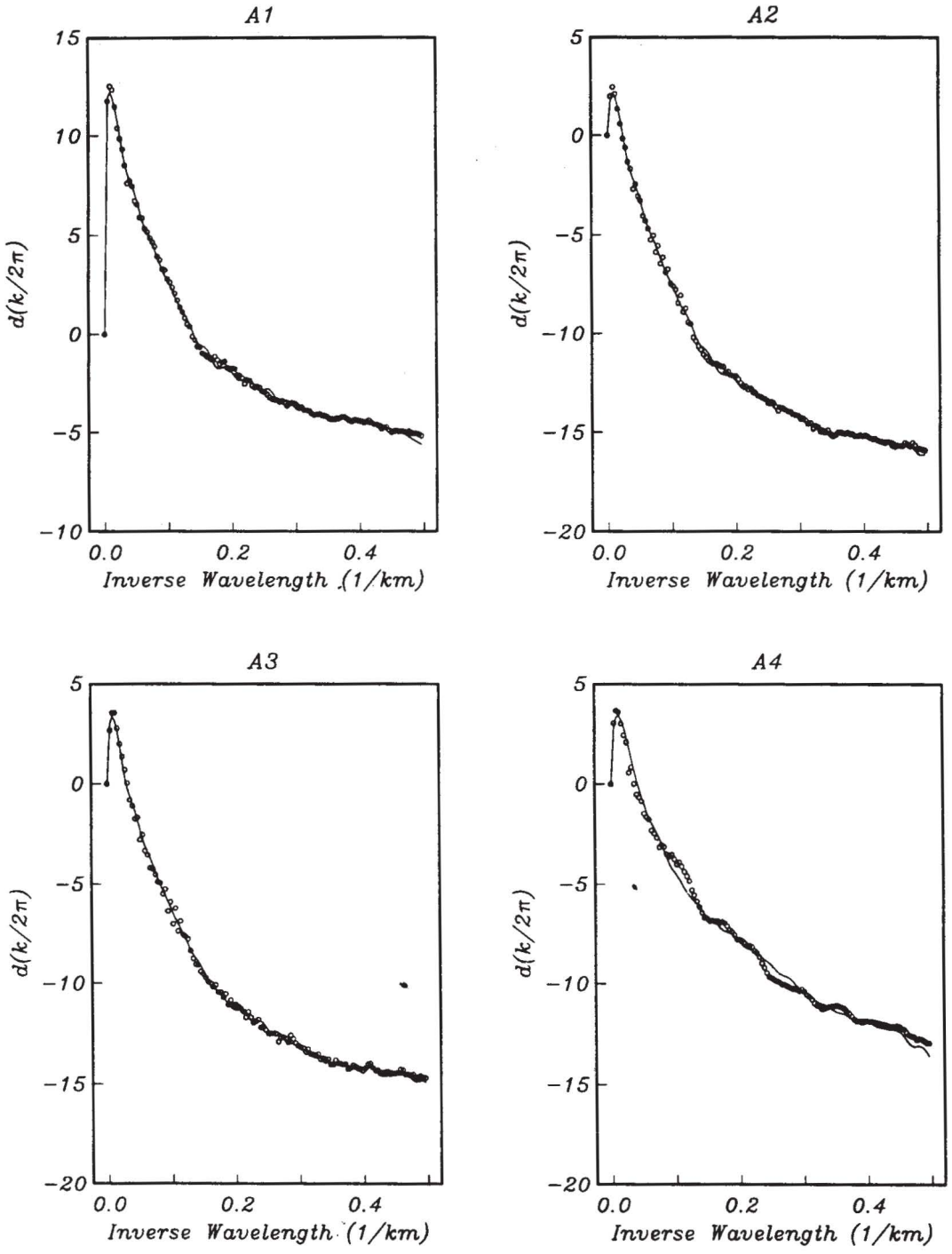

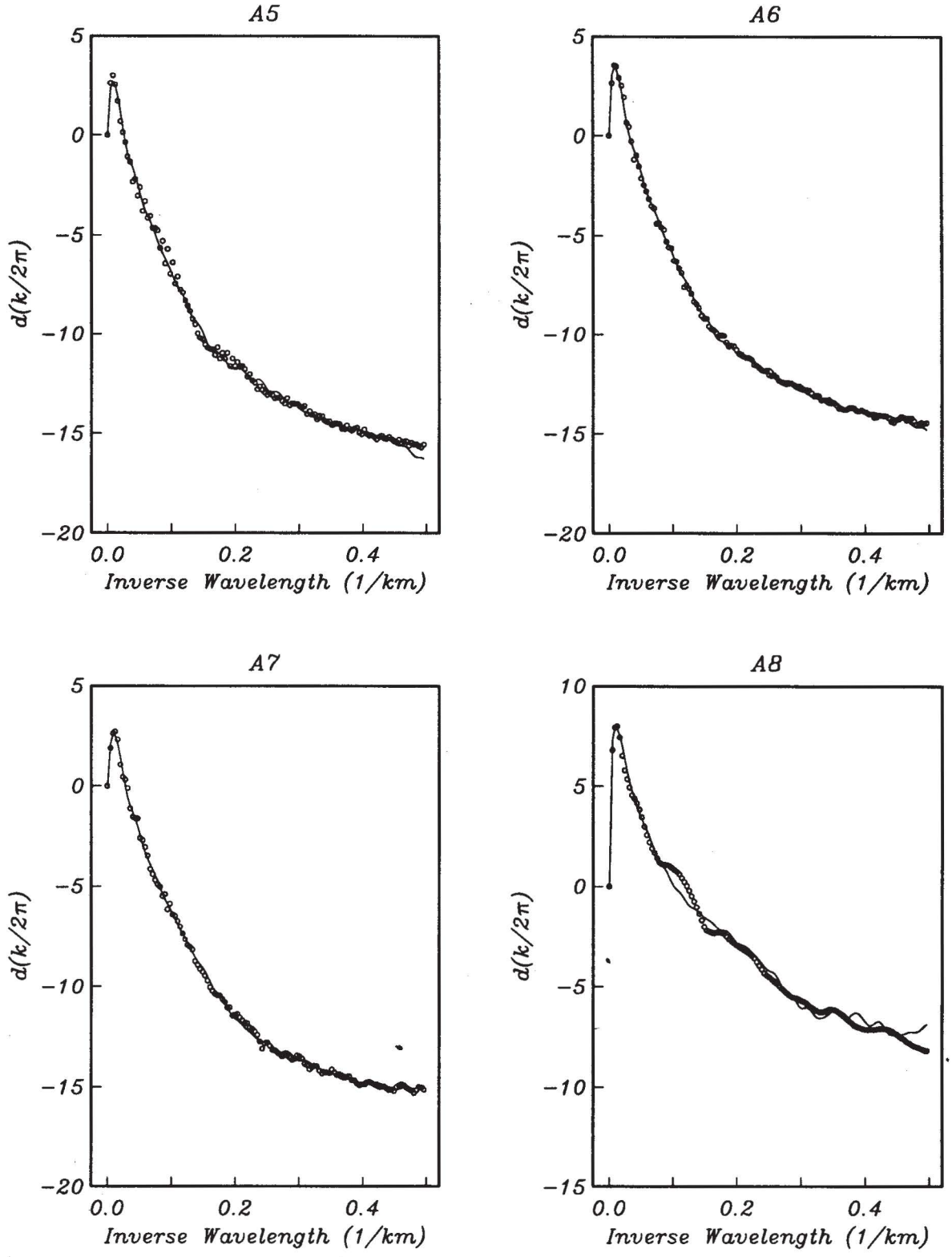
A5
A6
A7
A8
d(k/2π)
Inverse Wavelength (1/km)
0.0
0.2
0.4
5
0
-5
-10
-15
-20
10

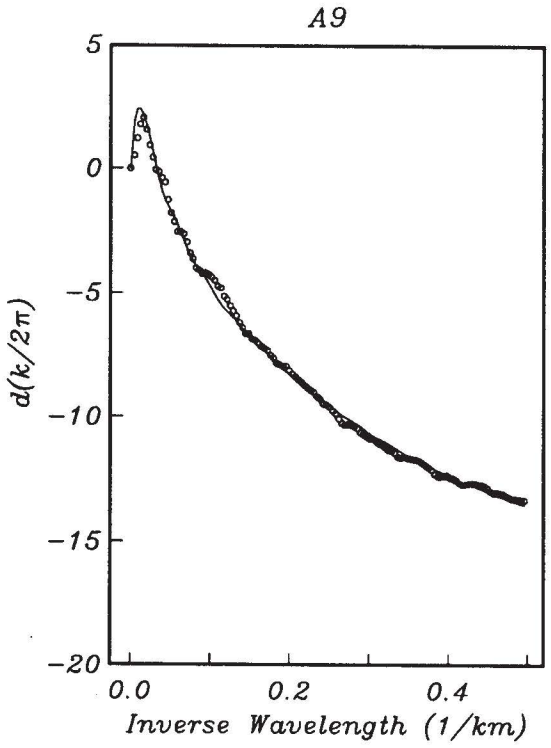
A9
5
0
-5
-10
-15
-20
d(k/2π)
0.0
0.2
0.4
Inverse Wavelength (1/km)

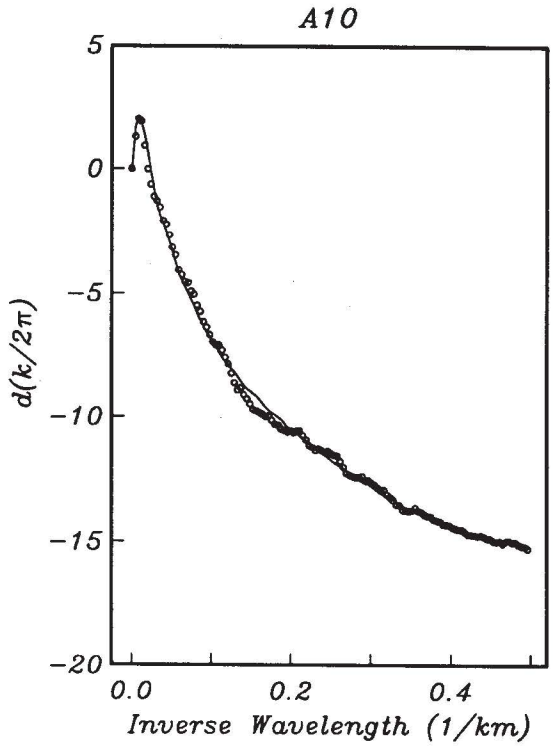
A10
5
0
-5
-10
-15
-20
d(k/2π)
0.0
0.2
0.4
Inverse Wavelength (1/km)

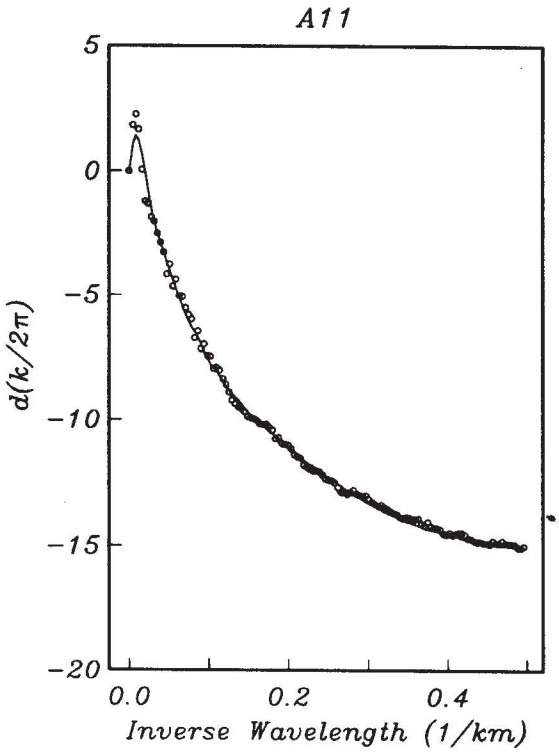
A11
5
0
-5
-10
-15
-20
d(k/2π)
0.0
0.2
0.4
Inverse Wavelength (1/km)

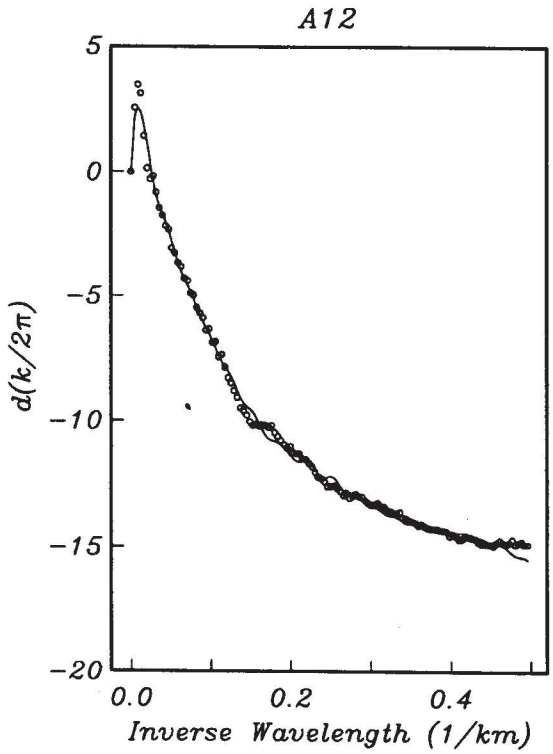
A12
5
0
-5
-10
-15
-20
d(k/2π)
0.0
0.2
0.4
Inverse Wavelength (1/km)

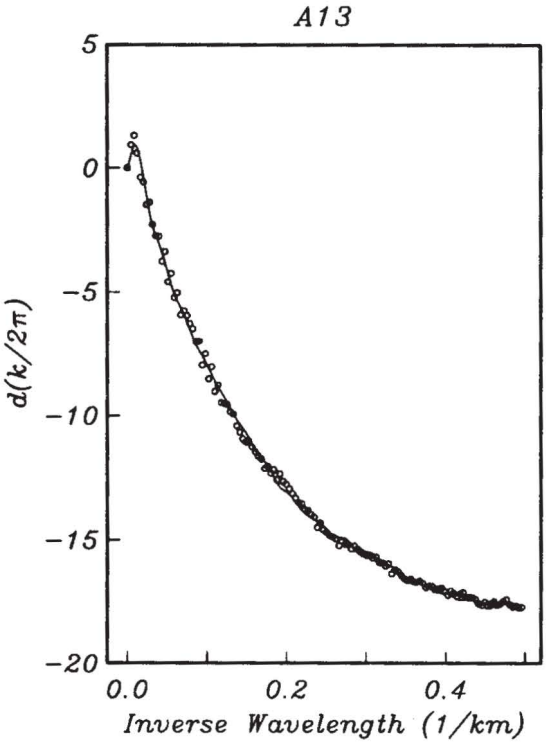
A13
5
0
−5
−10
−15
−20
d(k/2π)
0.0
0.2
0.4
Inverse Wavelength (1/km)

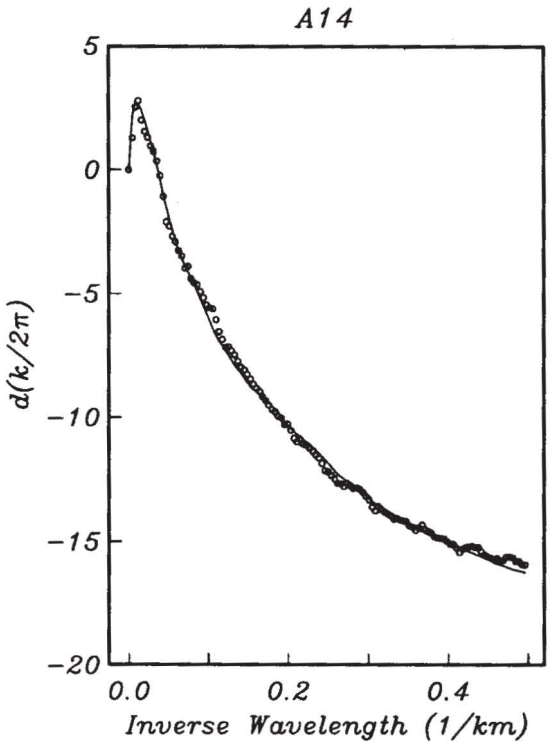
A14
5
0
−5
−10
−15
−20
d(k/2π)
0.0
0.2
0.4
Inverse Wavelength (1/km)

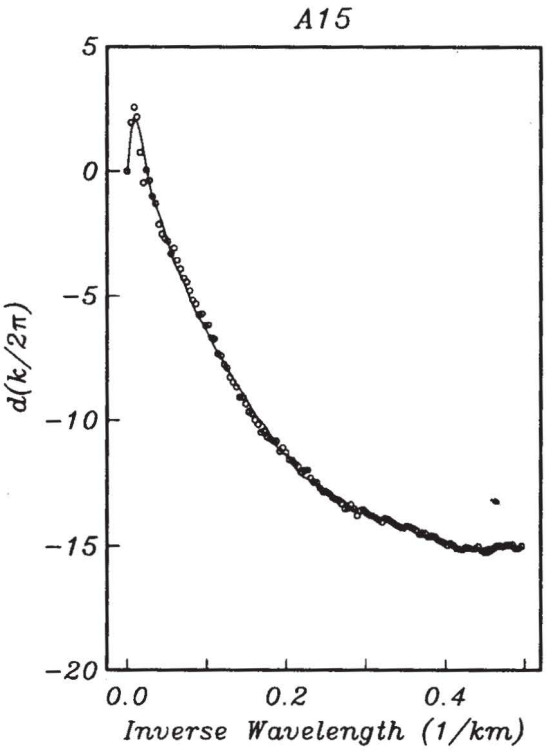
A15
5
0
−5
−10
−15
−20
d(k/2π)
0.0
0.2
0.4
Inverse Wavelength (1/km)

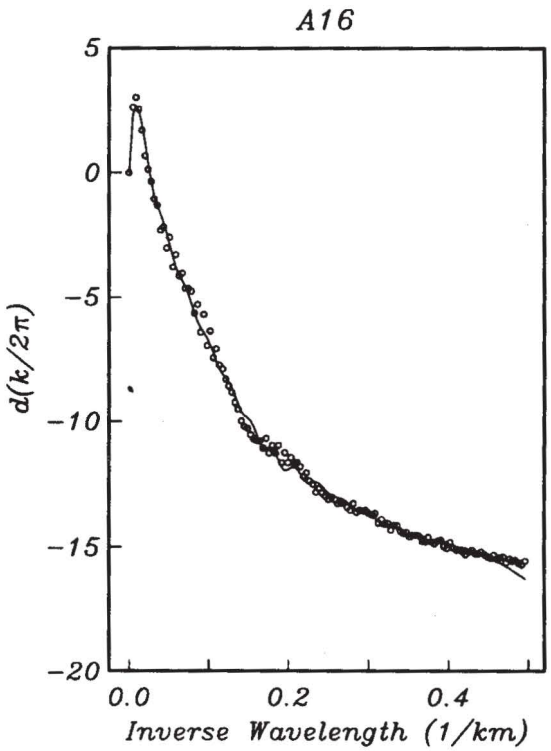
A16
5
0
−5
−10
−15
−20
d(k/2π)
0.0
0.2
0.4
Inverse Wavelength (1/km)

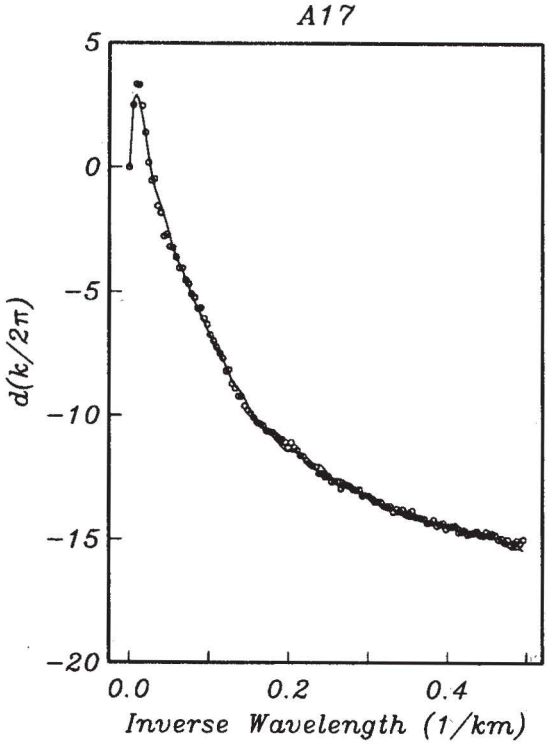
A17
5
0
-5
-10
-15
-20
d(k/2π)
0.0
0.2
0.4
Inverse Wavelength (1/km)

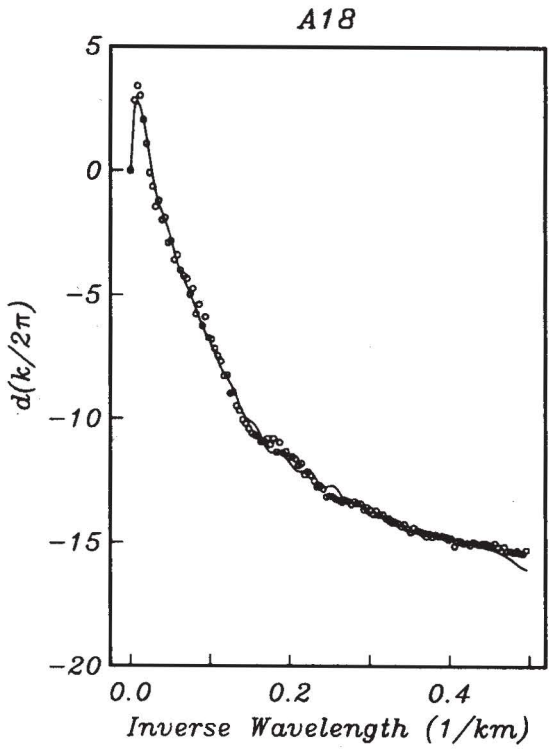
A18
5
0
-5
-10
-15
-20
d(k/2π)
0.0
0.2
0.4
Inverse Wavelength (1/km)

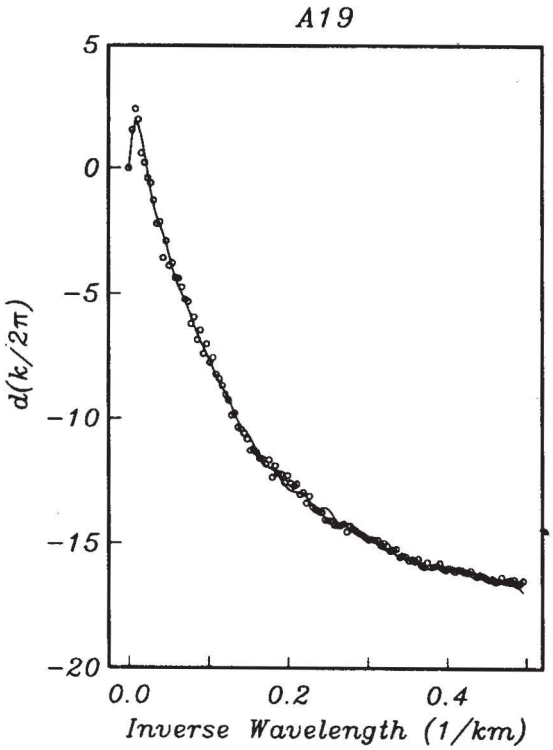
A19
5
0
-5
-10
-15
-20
d(k/2π)
0.0
0.2
0.4
Inverse Wavelength (1/km)

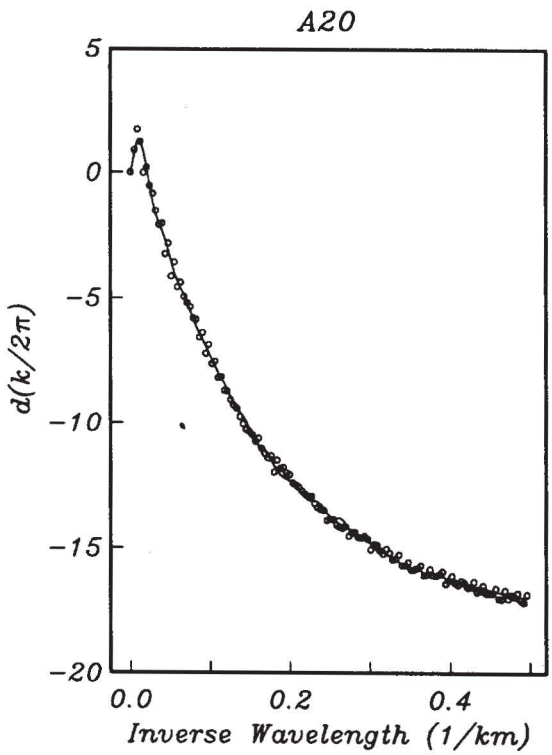
A20
5
0
-5
-10
-15
-20
d(k/2π)
0.0
0.2
0.4
Inverse Wavelength (1/km)

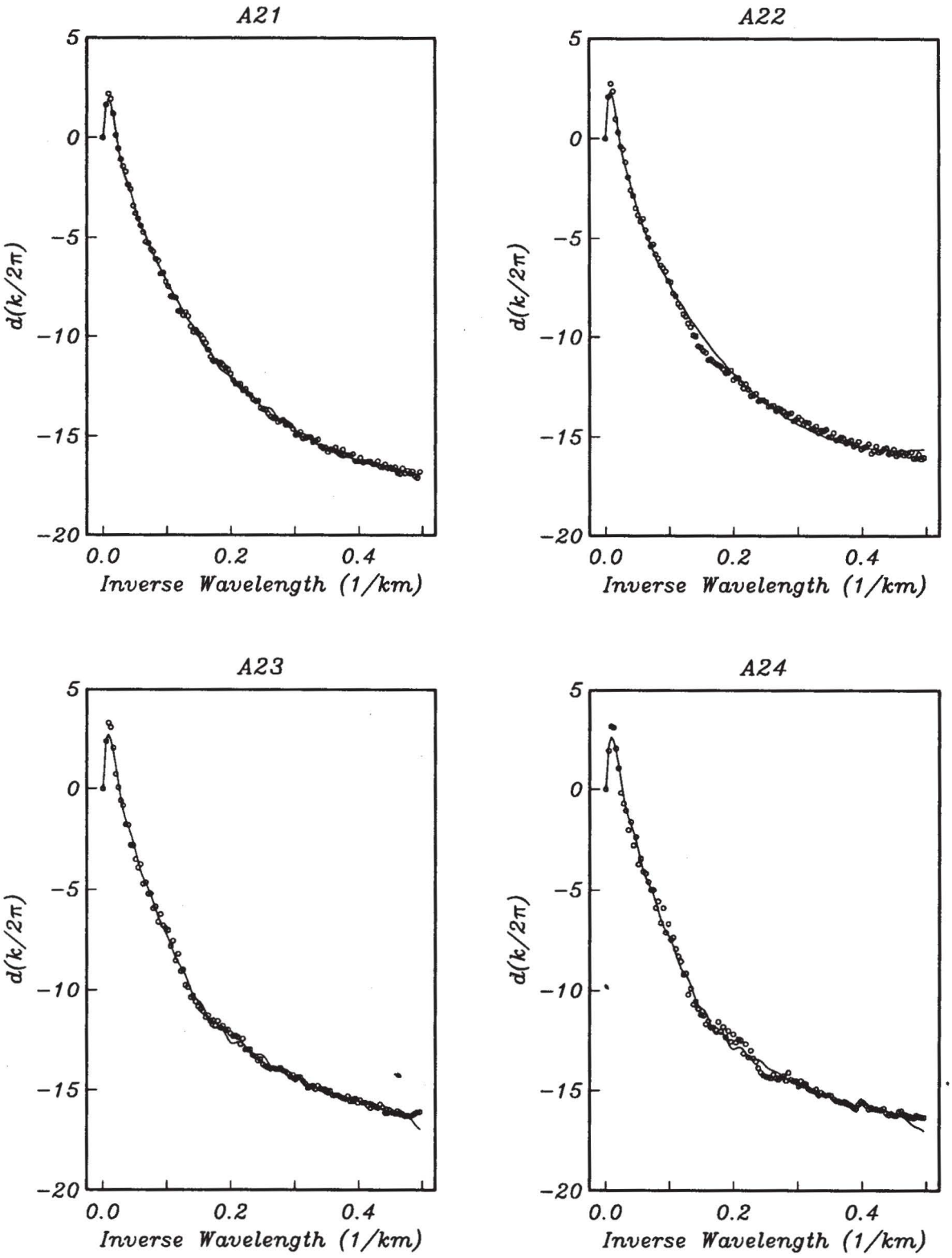
A21
A22
A23
A24
5
0
−5
−10
−15
−20
d(k/2π)
0.0
0.2
0.4
Inverse Wavelength (1/km)

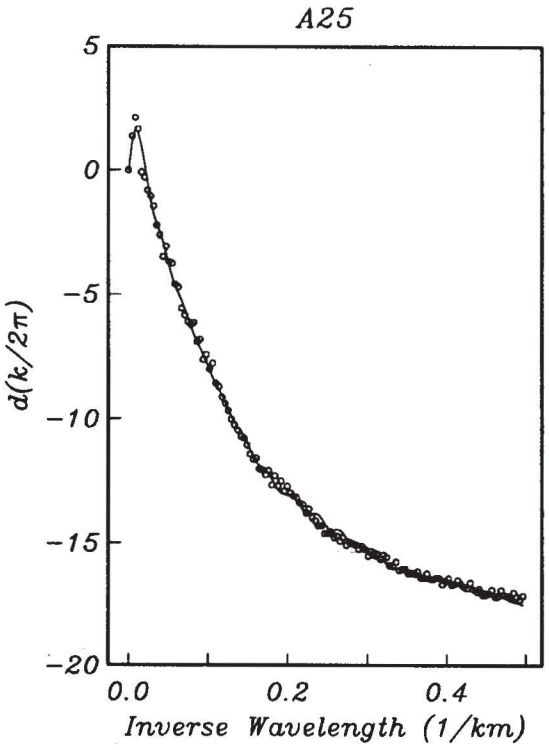
A25
5
0
−5
−10
−15
−20
d(k/2π)
0.0
0.2
0.4
Inverse Wavelength (1/km)

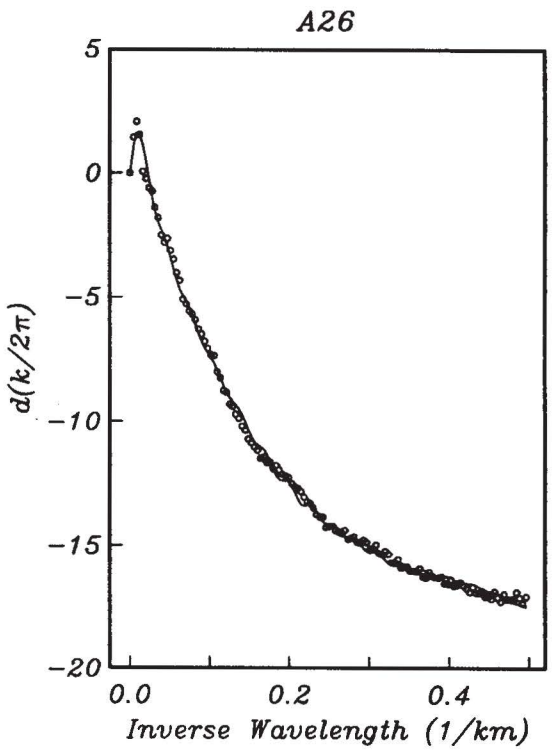
A26
5
0
−5
−10
−15
−20
d(k/2π)
0.0
0.2
0.4
Inverse Wavelength (1/km)

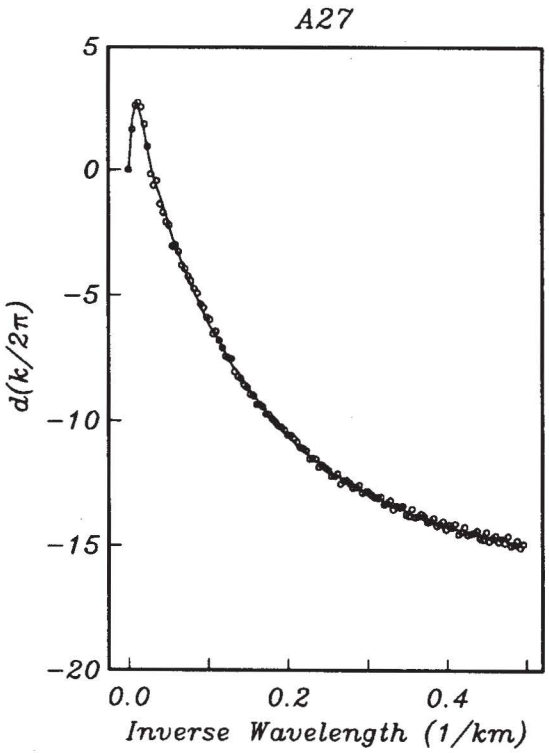
A27
5
0
−5
−10
−15
−20
d(k/2π)
0.0
0.2
0.4
Inverse Wavelength (1/km)

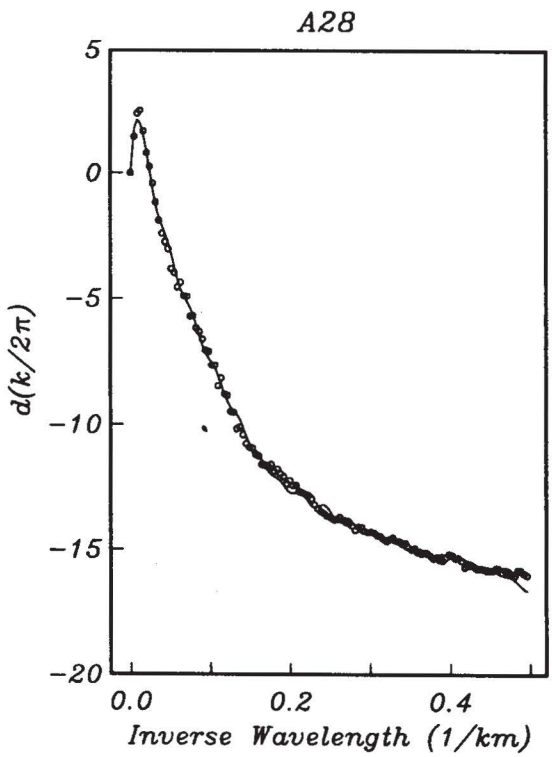
A28
5
0
−5
−10
−15
−20
d(k/2π)
0.0
0.2
0.4
Inverse Wavelength (1/km)

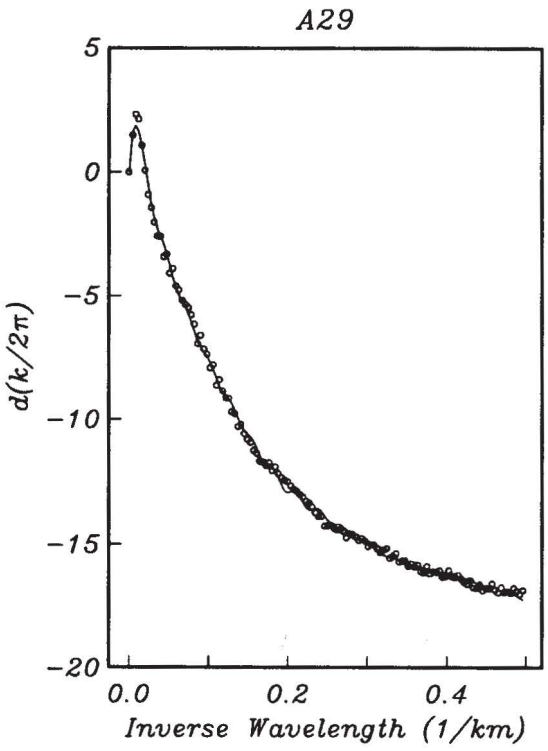
A29
5
0
−5
−10
−15
−20
d(k/2π)
0.0
0.2
0.4
Inverse Wavelength (1/km)

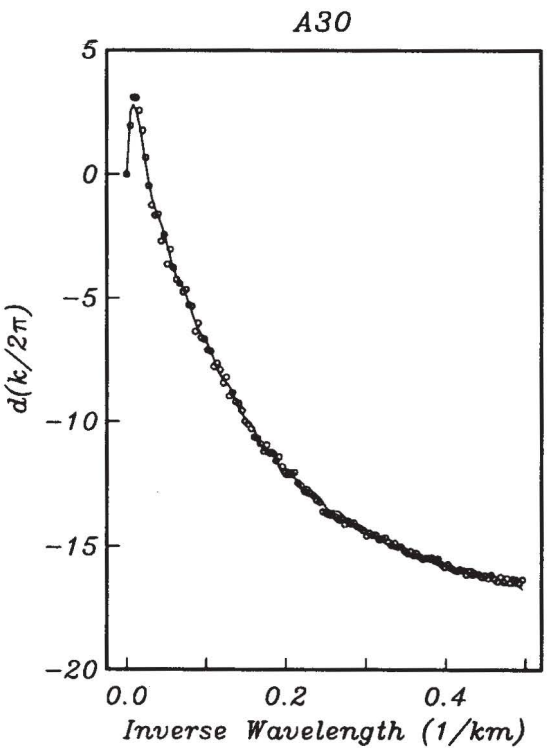
A30
5
0
−5
−10
−15
−20
d(k/2π)
0.0
0.2
0.4
Inverse Wavelength (1/km)

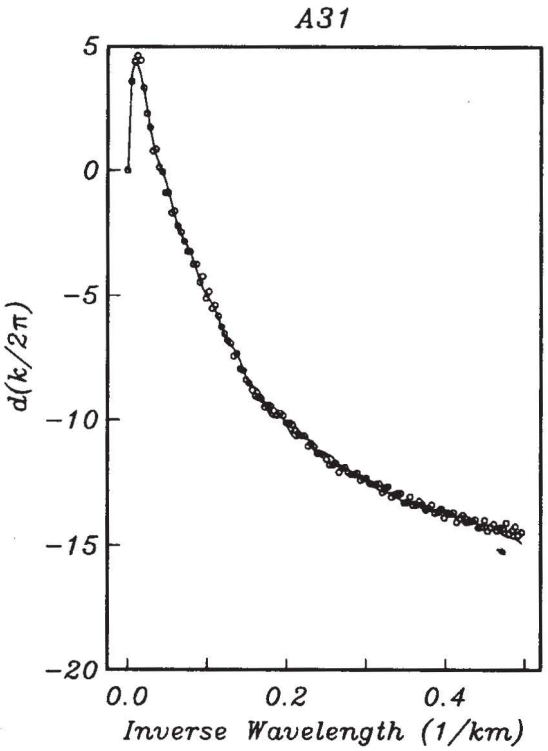
A31
5
0
−5
−10
−15
−20
d(k/2π)
0.0
0.2
0.4
Inverse Wavelength (1/km)

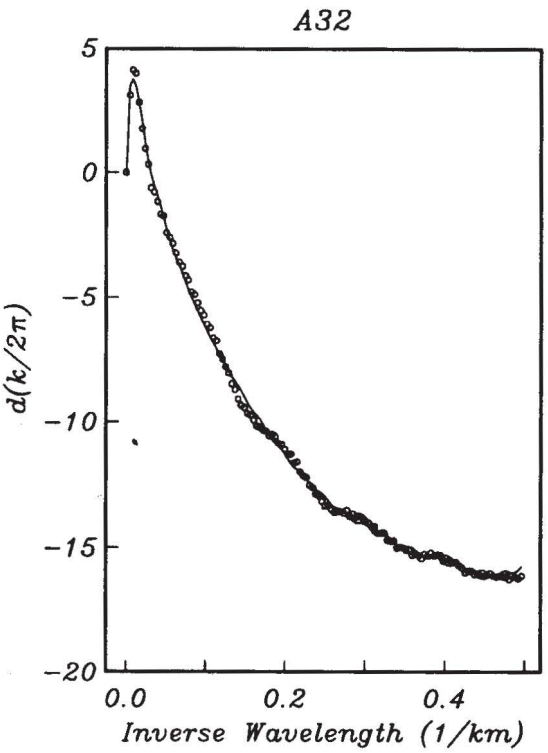
A32
5
0
−5
−10
−15
−20
d(k/2π)
0.0
0.2
0.4
Inverse Wavelength (1/km)

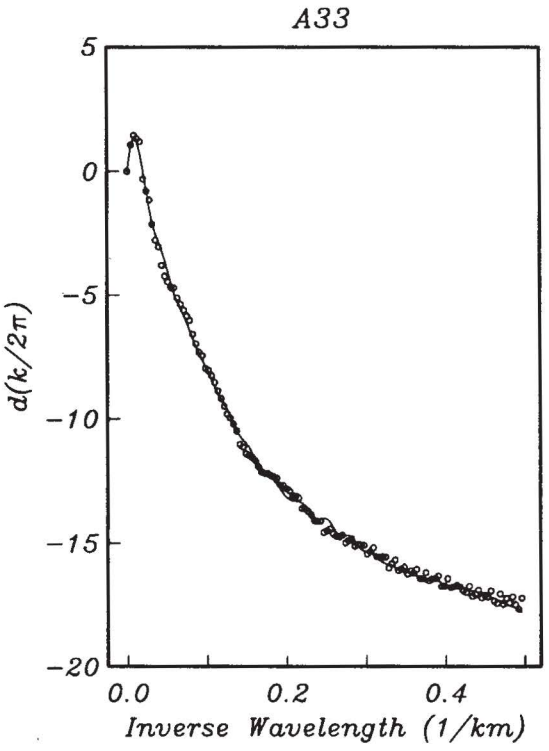

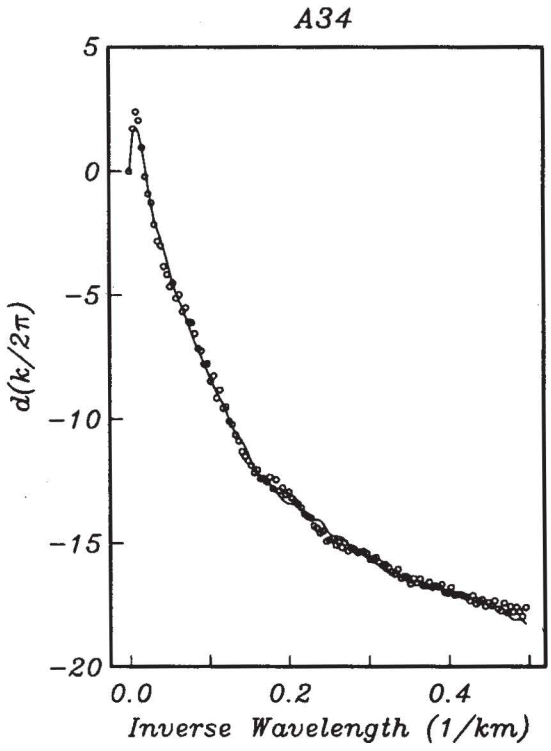

BIBLIOGRAPHY

ALVARADO-OMANA, M. A., 1986. Gravity and crustal structure of the south-central Gulf of Mexico, the Yucatán Peninsula and adjacent areas. M.S. Thesis, Oregon State University, Corvallis, Oregon.

ANTOINE, J. and J. EWING, 1963. Seismic refraction measurements on the margins of the Gulf of Mexico. *J. Geophys. Res., 68,* 1975-1996.

BHATTACHARYYA, B. K., 1966. Continuous spectrum of the total magnetic field anomaly due to a rectangular prismatic body. *Geophysics, 29,* 517-553.

BRIGGS, I. C., 1974. Machine contouring using minimum curvature. *Geophysics, 39,* 39-48.

BUFFLER, R. T., 1991. Seismic stratigraphy of the deep Gulf of Mexico basin and adjacent margins. *In:* The Geology of North America, Vol. J, The Gulf of Mexico Basin, The Geological Society of America.

CONEY, P. J. and M. F. CAMPA, 1983. Tectono-stratigraphic terranes and mineral resource distributions in Mexico. *Can. J. Earth Sci., 20,* 1040-1051.

DILLON, W. P. and J. G. VEDDER, 1973. Structure and development of the continental margin of British Honduras. *Geol. Soc. Am. Bull., 84,* 2713-2732.

EWING, J., J. ANTOINE and M. EWING, 1960. Geophysical measurements in the western Caribbean Sea and in the Gulf of Mexico. *J. Geophys. Res., 65,* 4087-4126.

GARCIA-ABDESLEM, J. and G. E. NESS, 1989. Spectral analysis and ridge-regression of magnetic anomalies. *In:* Expanded Abstracts of the Technical Program with Author's Biographies, 59th Annual International Meeting and Exposition, Society of Exploration Geophysicists, v 1, 308-311.

GARCIA-ABDESLEM, J., 1990. Spectral analysis and rigde-regression of magnetic anomalies from the northerm continental margin of the Yucatán Peninsula, Mexico, Ph. D. Thesis, Oregon State University, Corvallis, Oregon.

GARCIA-ABDESLEM, J. and G. E. NESS, 1994. Inversion of the power spectrum from magnetic anomalies. *Geophysics, 59,* 391-401.

HILDEBRAND, A.R., G. T. PENFIELD, D. A. KRING, M. PILKINGTON, A. CAMARGO-Z. and W. V. BOYNTON, 1991. Chicxulub Crater: A possible Cretaceous Tertiary boundary impact crater in the Yucatán Peninsula, Mexico. *Geology, 19,* 867-871.

IAGA (International Association of Geomagnetism and Aeronomy), 1986, International Geomagnetic Reference Field Revision 1985. *Geophysics, 51,* 1020-1023.

IBRAHIM, A.K., J. CARYE, G. V. LATHAM and R. T. BUFFLER, 1981. Crustal structure in Gulf of Mexico from OBS refraction and multichannel reflection data. *AAPG Bull., 65,* 1207-1229.

LOCKER, S.D. and R. T. BUFFLER, 1983, Comparisons of Lower Cretaceous carbonate shelf margins, northern Campeche Escarpment and northern Florida Escarpment, Gulf of Mexico. *In:* A.W. Bally (ed.), Seismic Expression of Structural Styles - A picture and Work Atlas: AAPG Studies in Geology No. 15, v. 2.

LOPEZ-RAMOS, E., 1975. Geological summary of the Yucatán Peninsula. *In:* A.F.M. Nair, and F.G. Stehli (ed.), The Ocean Basins and Margins, V. 3, 257-282, Plenum, New York.

MARQUARDT, D. W., 1963. An algorithm for least-squares estimation of nonlinear parameters. *J. Soc. Indust. Appl. Math., 11*, 431-441.

NESS, G.E., J. P. DAUPHIN, J. GARCIA-ABDESLEM and M. A. ALVARADO-OMANA, 1991. Bathymetry and Gravity and Magnetic Anomalies of the Yucatán Peninsula and Adjacent Areas: Geological Society of America, Map and Chart Series MCH073, Boulder, Colorado.

PENFIELD, G. T. and A. CAMARGO-Z., 1981. Definition of a major igneous zone in the central Yucatán platform with aeromagnetics and gravity. *In:* Technical Program, Abstracts and Biographies, 51st Annual International Meting, Society of Exploration Geophysicists, p. 37.

PINDELL, J.L., 1985. Alleghenian reconstruction and subsequent evolution of the Gulf of Mexico, Bahamas, and Proto-Caribbean. *Tectonics, 4*, 1-39.

SALVADOR, A., 1987. Late Triassic-Jurassic paleogeography and origin of the Gulf of Mexico basin. *AAPG Bull., 71*, 419-451.

SCHLAGER, W.T., R. T. BUFFLER *et al.*, 1984. Deep sea drillling proyect, Leg 77, southeastern Gulf of Mexico. *Geol. Soc. Amer. Bull., 95*, 226-236.

VINIEGRA-O., F., 1981. Great carbonate bank of Yucatán, southern Mexico. *J. Petroleum Geology, 3*, 247-278.

WINKER, C. D. and R. T. BUFFLER, 1984. Cross section Texas-Louisiana to Yucatán. *In:* R.T. Buffler, S.D. Locker, W.R. Bryant, S.A. Hall, and R.H. Pliger (ed): the Ocean Margin Drilling Program - Regional Data Synthesis Series, Atlas 6, Gulf of Mexico, Marine Science International.

J. García-Abdeslem[1] and G.E. Ness[2]

[1] *CICESE, División de Ciencias de la Tierra, Depto. de Geofísica Aplicada, Km. 109 Carretera Tijuana-Ensenada, 22860 Ensenada B. C., México.*

[2] *College of Oceanography, Oregon State University Corvallis, Oregon, 97331 USA*

[3] *Present address: Seafloor Surveys International, Inc., Pier 69, 2727 Alaskan Way, Seattle, Washington 98121 USA.*